ARTICLE IN PRESS

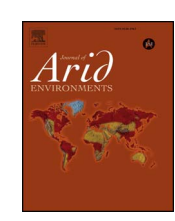
Journal of Arid Environments xxx (xxxx) xxx-xxx

FISEVIER

Contents lists available at ScienceDirect

Journal of Arid Environments

journal homepage: www.elsevier.com/locate/jaridenv



Simulated dynamics of soil water and pore vapor in a semiarid sandy ecosystem

Shohreh Pedram^a, Xixi Wang^{a,*}, Tingxi Liu^b, Limin Duan^b

- a Department of Civil and Environmental Engineering, Old Dominion University, Norfolk, VA 23529-0241, USA
- b College of Water Conservancy and Civil Engineering, Inner Mongolia Agricultural University, Hohhot, Inner Mongolia Autonomous Region 010018, China

ARTICLE INFO

Keywords: Dry soil layer Evaporation zone Heat transfer HYDRUS Soil evaporation

ABSTRACT

Understanding dynamics of soil water content (SWC) and pore air relative humidity (RH_{pa}), as influenced by wetting-drying cycles, is crucial for sustaining fragile ecosystems of desert lands across the world. However, to date, such an understanding is still incomplete. The objective of this study was to examine such dynamics at a typical desert site within the Horqin Sandy Land, located in Mongolian Plateau of north China. The results indicated that vaporization primarily occurred at a depth of around 10 cm below the ground surface. The diurnal variations of the SWC and RH_{pa} in the top 10 cm soils were much larger than those in the soils at a deeper depth. For a non-rainy day, the SWC and RH_{pa} were mainly determined by the relative magnitude of atmospheric temperature over soil temperature, whereas, for a rainy day, the SWC and RH_{pa} were primarily controlled by the rainfall pattern and amount. The retardation role of the top dry soil layer, which is about 10 cm thick and exists most time at the study site, can effectively prevent the beneath moist soils from being further dried up, and thus is beneficial for sustaining the desert ecosystem.

1. Introduction

In arid/semiarid regions, where the hydrologic cycle is dominated by vertical water movement (i.e., soil water evaporation) as influenced by heat transport (Dong et al., 2003; Wang, 2015), soil water content (SWC) and pore air humidity (RHpa) are two important indicators of available water for sustaining their fragile sparse vegetation ecosystems (Goss and Madliger, 2007; Duan et al., 2011, 2015). Hereinafter, SWC is defined as the ratio of soil water volume to bulk soil volume, while RH_{pa} is defined as the ratio of the partial pressure of water vapor to the total pressure of air in soil pores (Farouki, 1981). When transported into soils, heat will cause increase of soil temperature, vaporizing soil water into pore vapor, in reverse, when soil temperature is cooled down, pore vapor can be condensed back into soil water (Wang, 2015). The heat emission out of soils will not only lower soil temperature but also cause loss of pore vapor to the ambient atmosphere (i.e., soil evaporation). For an area of interest, when such a vaporization-condensation dynamic process becomes insufficient to meet the water demand of sparse vegetation, this area will likely be subject to desertification. As a major reason for land deterioration in the arid regions of the world (Kassas, 1995; Zucca et al., 2011), including the Horqin Sandy Land (HSL) of Eurasian Grassland, desertification is closely related to the increasing soil evaporation as a result of inappropriate land management practices (e.g., removal of native grasses and plantation of deep-root trees) (Zhao et al., 2010; Smits et al., 2012; Wang, 2015; Li et al., 2016a). In order to develop practical measures for solving desertification-related eco-environmental problems (e.g., dust storm and loss of grassland production), it is needed to have a good understanding of soil water and pore vapor dynamics.

As noted by previous studies (e.g., Wang et al., 2006; Liu et al., 2013), such an understanding can be challenging because of the twophase (i.e., liquid-vapor) fluid condition and the vapor flow resistance (VFR) effect of a thin (5-10 cm) top dry soil layer (DSL). The semiarid regions are usually dominated by bare sandy soils with such a DSL most of the time, within which soil moisture is dominantly in vapor phase with a very large capillary suction head (> 15,000 cm water height) (Goss and Madliger, 2007). In the past two decades, various laboratory and field studies (e.g., Daamen and Simmonds, 1996; Yamanaka and Yonetani, 1999; Saravanapavan and Salvucci, 2000; Wang et al., 2006; Goss and Madliger, 2007; Novak, 2010; Sakai et al., 2011; Liu et al., 2013) have been conducted to measure soil evaporation in water-limited environment. However, most of the studies were for short-term periods (i.e., from several days to a few months) and rarely measured vertical profiles of SWC and soil temperature, making it hard to determine dynamics of soil water and pore vapor as influenced by wetting-drying cycles. On the other hand, a few studies (e.g., Yamanaka

E-mail addresses: spedr002@odu.edu (S. Pedram), xxqqwang@gmail.com (X. Wang), txliu@imau.edu.cn (T. Liu), dlm@imau.edu.cn (L. Duan).

https://doi.org/10.1016/j.jaridenv.2017.11.004

Received 12 February 2017; Received in revised form 12 October 2017; Accepted 10 November 2017 0140-1963/ Published by Elsevier Ltd.

^{*} Corresponding author.

S. Pedram et al.

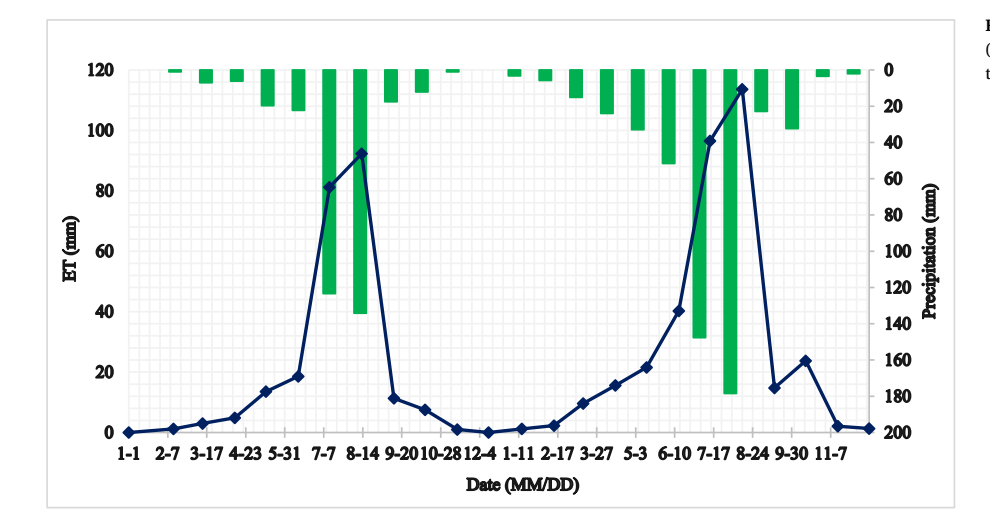


Fig. 1. Monthly precipitation and actual evapotranspiration (AET) at the study site. Each bar/dot represents a month of the plotting date.





Fig. 2. Pictures of the: (a) plane view (with the sensorbased weather station tower); and (b) soil vertical profile (with three-needle heat pulse or TNHP sensors), of the study site.

Table 1
Precipitation and rainy days in each month of the two study years.

Year		ation (mm) er of Rainy D	Days)										
	Jan	Feb	Mar	Apr	May	Jun	Jul	Aug	Sep	Oct	Nov	Dec	Annual
2013	0 (0)	1.1 (2)	7.1 (3)	6.2 (3)	19.7 (5)	22.3 (5)	123.4 (9)	134.2 (11)	17.6 (3)	12.2 (4)	1.1 (2)	0 (0)	344.9 (47)
2014	3.3 (4)	5.8 (5)	15.1 (5)	24.0 (6)	33.7 (6)	51.6 (3)	147.7 (4)	178.5 (7)	22.9 (5)	32.4 (4)	3.5 (2)	2.1 (1)	520.6 (52)

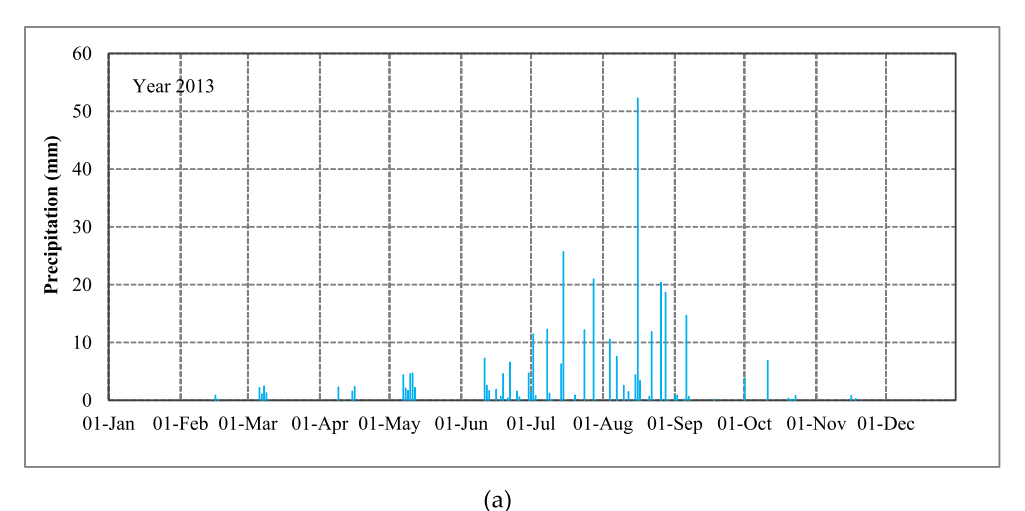
et al., 1998; Sakai et al., 2011) used mathematical models to reproduce the vaporization-condensation-movement dynamics observed in laboratory soil columns, without determining the dynamics of soil water and pore vapor within different soil layers. Wang (2015), the correspondence author of this paper, conducted an overview of existing studies attempting to measure and/or model soil water evaporation in arid/semiarid environment, concluding that to fill the knowledge gap of soil water and pore vapor dynamics, field measurements need to be extrapolated using mathematical models.

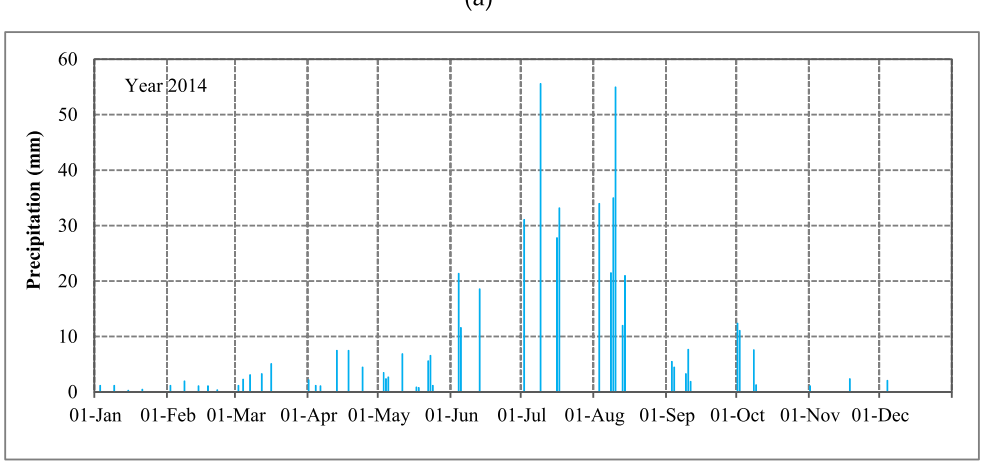
The liquid-heat-vapor processes in a soil profile can be described by the Philip and de Vries (1957) theory (hereinafter designated as the PdV for description purposes), which in turn can be modeled using a set of partial differential equations. In reality, these processes interactively determine the soil evaporation phase at any time of interest. Philip (1958) classifies the desiccation of a soil profile into three phases (i.e., Phase I to III). Phase I occurs when the soil is sufficiently moist and thus has a soil water evaporation (E) indistinguishable from that with saturated surface (E_s), whereas, Phase III occurs when the soil surface

layers are very dry and E is sensitive to, and may be negatively correlated with, heat flux into soil. Phase II occurs when the soil has an intermediate moisture content and thus E is independent of $E_{\rm s}$ and depends on soil moisture distribution only. During Phase I, liquid water is supplied from the lower layers and vaporized at the soil surface at rate $E_{\rm s}$, and then the vapor is transferred into the ambient atmosphere. On the other hand, during Phase II and III, vaporization takes place not at the surface but within the soil mass (e.g., the evaporation zones or EZs), and the vapor diffuses upward through a top DSL to the surface and then into the atmosphere. Such classification of evaporation phases is verified by field observations presented by Goss and Madliger (2007).

Based on a few previous studies (e.g., Yamanaka and Yonetani, 1999; Goss and Madliger, 2007), during Phase I and II, E tends to be maximal when total heat flux into the soil is greatest (e.g., at noon), whereas, during Phase III, E tends to be maximal when total heat flux out of the soil is greatest (e.g., at midnight), and vice versa. This is because for Phase I and II, liquid water is vaporized at/near soil surface, which is positively related to the solar radiation (i.e., heat) input into

Fig. 3. The daily precipitations in year: (a) 2013; and (b) 2014.





(b)

Table 2
Ranges and adopted values of the HYDRUS-1D parameters in this study.

Parameter	Definition	Range ^a	Adopted Value
$\alpha [cm^{-1}]^b$	Parameter in the soil water retention function	0.029-0.70	0.147
n [-] ^b	Parameter in the soil water retention function	2.0-6.95	1.34
Q _r [-]	Residual soil water content	0.0 – 0.1	0.02
Q _s [-]	Saturated soil water content	0.35-0.45	0.38
K_s [cm d ⁻¹]	Saturated hydraulic conductivity	200-1520	650
I [-]	Tortuosity parameter in conductivity function	0.3–1.0	0.5

^a Determined from our decades-long laboratory experimental results (Duan et al., 2011) and literature (Ghanbarian-Alavijeh et al., 2010).

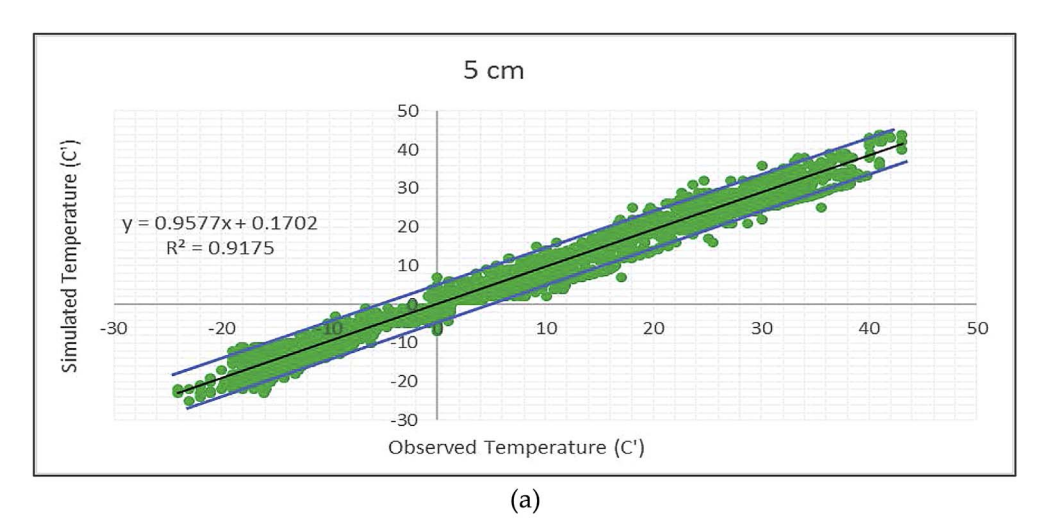
the soil. A larger heat input will prompt the desiccation of soil surface layer, increasing the upward suction gradient and thus facilitating the upward transport of liquid water. When the heat flux into the soil is greatest, the rates of desiccation and liquid upward movement will become fastest, leading to a maximal evaporation rate. In contrast, for Phase III, the vaporization occurs within the soil mass and then the vapor needs to be transported upward through the above dry soils into the ambient atmosphere. The transport of vapor is primarily driven by upward temperature gradients between a deeper and upper layer as well as between the top soil layer and the ambient atmosphere. When the heat flux out of the soil is greatest, the upward gradients will be

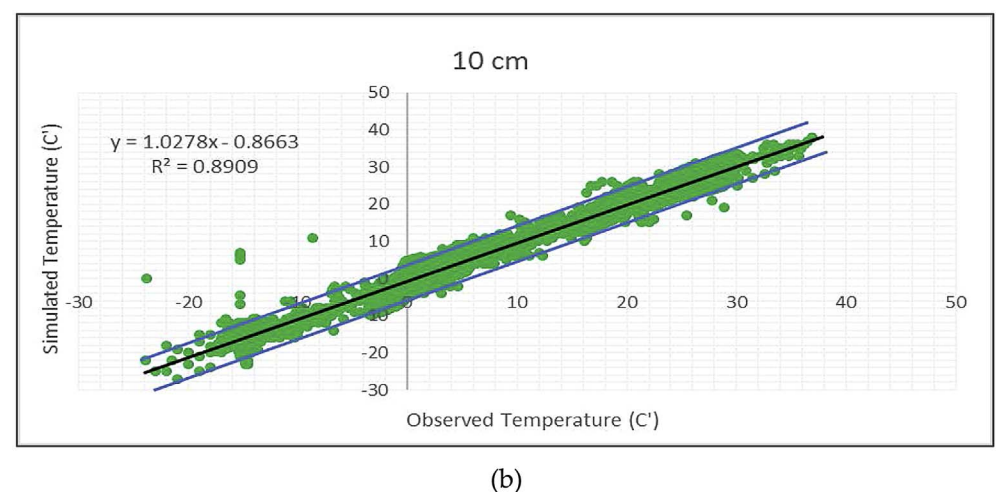
greatest and thus the E rate can reach a maximal value. However, because of wrong modeling premises (e.g., E monotonically increases with heat input) and/or insufficient and inclusive experimental (mostly laboratory soil-column) data (Goss and Madliger, 2007; Wang, 2015), previous studies (van Bavel and Hillel, 1976; Mahfouf and Noilhan, 1991; Kondo et al., 1992; Bristow and Horton, 1996; Yamanaka et al., 1998; Yamanaka and Yonetani, 1999; Saravanapavan and Salvucci, 2000; Mori et al., 2003; Gowing et al., 2006; Saito et al., 2006; Heitman et al., 2008; Novak, 2010; Liu, 2011; Sakai et al., 2011; Xiao et al., 2011; Shahraeeni et al., 2012) primarily examined and reported dynamics of Phase I and II evaporation. For this reason, the features presented by those studies are unlikely to be found at any sites under naturally dry conditions (e.g., desert regions), where most of the time a top DSL overlies underlying moist soils and Phase III dominates soil water evaporation process.

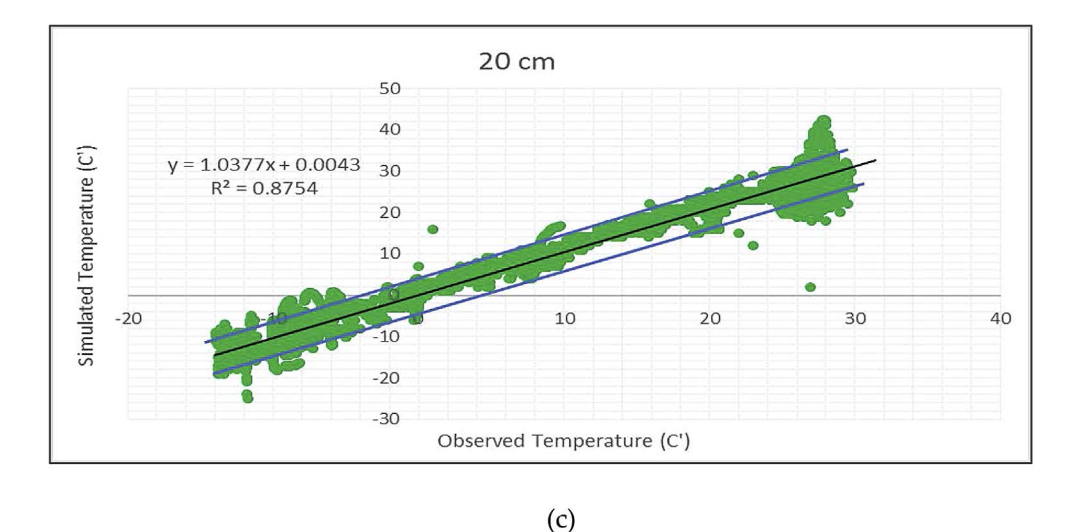
The advancement of heat pulse sensors in the past decade has made it possible for the PdV to be widely applied in practice to determine soil evaporation (Bristow et al., 1993; Liu et al., 2013; Kamai, 2013). Although the PdV has been programmed into a family of HYDRUS computer software packages (Šejna et al., 2011; Šimůnek et al., 2011), few applications in very dry regions, where Phase III soil evaporation dominates the hydrology cycle most of the time, have been reported in existing literature (Zeng et al., 2009, 2011a, b). The objective of this study was to examine the SWC and RH_{pa} dynamics in a desert sandy soil, as influenced by heating-cooling and wetting-drying cycles, by extrapolating field data on SWC and soil temperature using HYDRUS-1D. Such information is needed (but incomplete) for developing

^b The parameter of the van Genuchten (1980) model for soil water retention function.

Fig. 4. The HYDRUS-simulated versus measured soil temperatures at: (a) 5 cm; (b) 10 cm; (c) 20 cm depths below the ground surface. The thick black line is the linear regression line, the two thin blue lines are the 95% upper and lower confidence limits. (For interpretation of the references to colour in this figure legend, the reader is referred to the web version of this article.)







practical measures to protect/restore degrading or degraded sandy ecosystems in arid/semiarid environment.

2. Material and method

2.1. Description of HYDRUS-1D

HYDRUS-1D, which solves the PdV governing equation using a onedimensional finite-element scheme, was designed to model movement of water, heat, and multiple solutes in variably saturated porous media (Šimůnek and van Genuchten, 2008). It has a "freezing module" that represents hydrologic processes for the times when soil temperature is below the freezing point (Zhao et al., 2016). HYDRUS-1D is supported by an interactive graphics-based interface for data-preprocessing, discretization of the soil profile, and graphic presentation of the results. This study used the latest HYDRUS-1D code (ver. 4.16.010) that can compute $\mathrm{RH}_{\mathrm{pa}}$ using Equation (5).

The PdV governing equation solved by HYDRUS-1D can be

Table 3Performance measures of the HYDRUS-1D model for the calibration period (Jan. 1 to Dec. 31, 2013).

Depth below the Ground Surface (cm)	Soil Temp	erature				Soil Water	Content			
	Mean (°C)	Std. (°C)	C _v ^b	RRSME ^c	R ²	Mean	Std.	C _v ^b	RRSME ^c	R ²
5	6.55	2.33	0.35	0.112	0.91	0.0104	0.00123	0.11	0.113	0.90
	(7.45)	(3.44)	(0.46)			(0.0098)	(0.00122)	(0.12)		
10	5.45	1.88	0.34	0.129	0.89	0.0255	0.00103	0.066	0.128	0.89
	(6.66)	(2.04)	(0.30)			(0.0202)	(0.00108)	(0.10)		
20	7.55	1.02	0.13	0.133	0.87	0.056	0.00101	0.017	0.106	0.93
	(8.34)	(1.13)	(0.13)			(0.0435)	(0.00111)	(0.025)		
30	8.01	3.13	0.39	0.130	0.88	0.076	0.00055	0.0072	0.142	0.84
	(9.13)	(2.23)	(0.24)			(0.069)	(0.00101)	(0.014)		
40	8.83	3.44	0.38	0.202	0.79	0.094	0.00204	0.021	0.204	0.78
	(9.44)	(2.62)	(0.27)			(0.105)	(0.00345)	(0.032)		
50	9.02	3.02	0.33	0.145	0.83	0.106	0.0045	0.042	0.135	0.86
	(10.15)	(3.19)	(0.31)			(0.113)	(0.0048)	(0.043)		

^a The value in bracket is the measured.

expressed as (Saito et al., 2008):

$$\frac{\partial \theta}{\partial t} = -\frac{\partial q_{\rm L}}{\partial z} - \frac{\partial q_{\rm v}}{\partial z} - S \tag{1}$$

where $\boldsymbol{\theta}$ [-] is the volumetric soil water content (i.e., SWC); q_l [cm d $^{-1}$] is the net flux of liquid water; q_v [cm d $^{-1}$] is the net flux of vapor; \mathbf{t} [d] is the simulation time; \mathbf{z} [cm] is the vertical axis being positive downward; and \mathbf{S} [\mathbf{d}^{-1}] is either the soil water sink (negative) or loss (positive) term.

 $q_{\rm L}$ is computed as:

$$q_{L} = q_{Lh} + q_{LT} = -K_{Lh} \left(\frac{\partial h}{\partial z} + 1 \right) - K_{LT} \frac{\partial T}{\partial z}$$
(2)

where q_{Lh} [cm d⁻¹] is the isothermal liquid water flux; q_{LT} [cm d⁻¹] is the thermal liquid water flux; T [K] is the soil temperature; h [cm] is the matric potential head in water height; K_{Lh} [cm d⁻¹] is the isothermal liquid hydraulic conductivity; and K_{LT} [cm² K⁻¹ d⁻¹] is the thermal liquid hydraulic conductivity.

 q_v is computed as:

$$q_{\nu} = q_{\nu h} + q_{\nu T} = -K_{\nu h} \left(\frac{\partial h}{\partial z} \right) - K_{\nu T} \frac{\partial T}{\partial z}$$
(3)

where q_{vh} [cm d⁻¹] is the isothermal vapor flux; q_{vT} [cm d⁻¹] is the thermal vapor flux; K_{vh} [cm d⁻¹] is the isothermal vapor hydraulic conductivity; and K_{vT} [cm² K⁻¹ d⁻¹] is the thermal vapor hydraulic conductivity.

Substituting Equations (2) and (3) back into Equation (1), one can rewrite the PdV equation as:

$$\frac{\partial \theta}{\partial t} = \frac{\partial}{\partial z} \left[K_{Lh} \left(\frac{\partial h}{\partial z} + 1 \right) + K_{LT} \frac{\partial T}{\partial z} + K_{\nu h} \left(\frac{\partial h}{\partial z} \right) + K_{\nu T} \frac{\partial T}{\partial z} \right] - S$$

$$= \frac{\partial}{\partial z} \left[K_{Th} \left(\frac{\partial h}{\partial z} \right) + K_{Lh} + K_{TT} \frac{\partial T}{\partial z} \right] - S$$
(4)

where $K_{Th} = K_{Lh} + K_{vh}$ [cm d⁻¹] is the total isothermal hydraulic conductivity; and $K_{TT} = K_{vT} + K_{LT}$ [cm² K⁻¹ d⁻¹] is the total thermal hydraulic conductivity.

Based on the aforementioned definition of RH_{pa} and the ideal gas equation, Farouki (1981) derived a computational formula that is used in HYDRUS-1D. This formula can be expressed as:

$$RH_{pa} = Exp\left(\frac{h.\ Mg}{RT}\right) \tag{5}$$

where Exp() is the natural exponential function; M [= 0.018015 g mol⁻¹] is the molecular weight of water; g

[= 9.81 m s^{-2}] is the gravitational acceleration; and R [= $8.314 \text{ J mol}^{-1} \text{ K}^{-1}$] is the universal gas constant.

2.2. The study site

The study site (122°37′30" E, 43°20′56" N) is located within the 51,700 km² HSL (118°35′ to 123°30′ E, 42°41′ to 45°15′ N) (Wang, 2015). The HSL landscape features consist of sand dunes (55%), meadows (27%), farmlands (10%), lakes (5%) and residential areas (3%) (Duan et al., 2011). With a temperate and semiarid continental monsoonal climate, on average, this region receives 389 mm precipitation annually, of which 69.3% falls during the growing season (June to August), while it has a very high annual potential evapotranspiration (PET) of 1412 mm. Given that the PET is almost four times larger than the annual precipitation, the site is climatically semiarid. As a result, for a given month, the actual evapotranspiration (AET) is almost same as the precipitation (Fig. 1), that is, most precipitation is lost to evaporation. It has an average annual temperature of around 6.6 °C, with a minimum monthly mean temperature of -13.3 °C in January and a maximum temperature of 23.8 °C in July, and an average annual wind speed of 3.8 m s⁻¹, with a minimum monthly mean wind speed of 3.0 m s⁻¹ in August and a maximum of 5.0 m s⁻¹ in April. The prevalent wind direction is northwest in winter and spring, whereas, it is southwest in summer and fall.

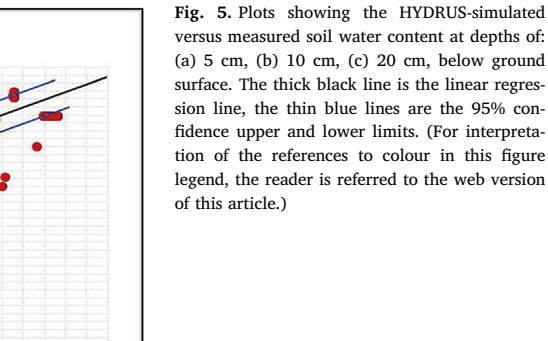
The study site is covered by nearly-bare desert sandy soils (Fig. 2) (Duan et al., 2011). From the ground surface to the depth of 80 cm, the soils (median porosity $Q_s=0.387$) are composed of 98.91% sand particles (diameter of 0.05–2.0 mm) and 1.09% silt particles (diameter of 0.002–0.05 mm), whereas, below the depth of 80 cm, the soils (median $Q_s=0.382$) are composed of 99.7% sand particles and 0.30% silt particles. The soils have no clay particles at all. The wilting point of the soils is 0.02 (Dong et al., 2003). The depth to water table at the study site is deeper than 4.0 m (Duan et al., 2015).

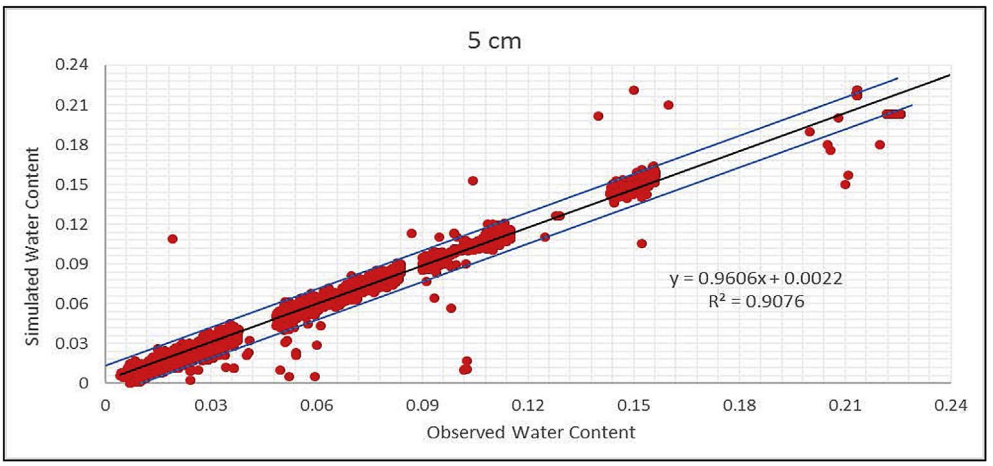
2.3. Instrumentation and data

A sensor-based weather station (Fig. 2a) at the study site was installed to continuously record data on precipitation, air temperature, relative humidity of the ambient air, wind speed and direction, solar radiation, and atmosphere vapor pressure. At the same time, relevant sensors were installed (as illustrated in Fig. 2b) to continuously measure soil moistures and soil temperatures at seven depths of 10, 20, 40, 80, 120, 160, and 200 cm. In addition, a three-needle heat pulse (TNHP) sensor was used to continuously measure temperatures and water contents of the surface (i.e., top 1 cm) soil. All data were

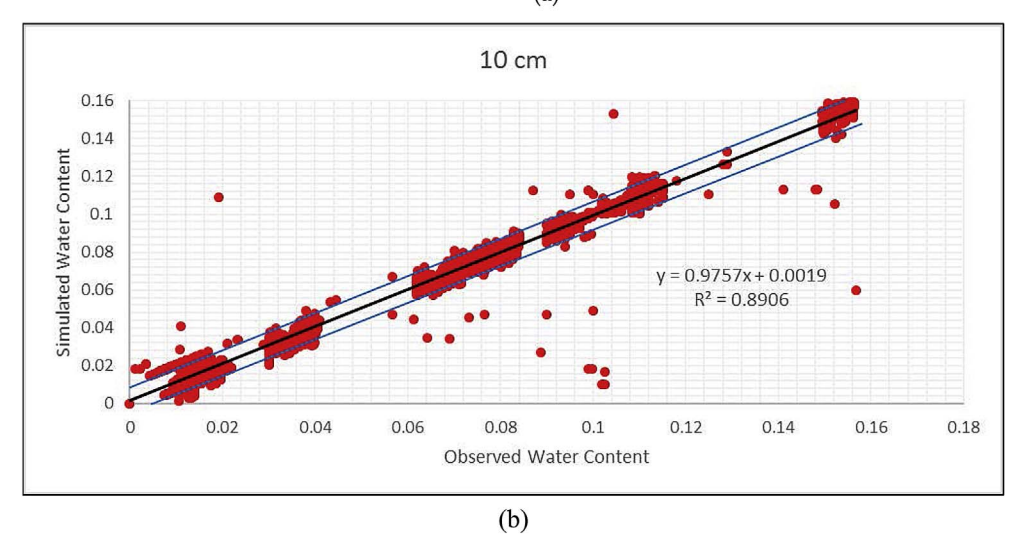
^b Coefficient of variation, defined as the ratio of standard deviation (Std.) to mean.

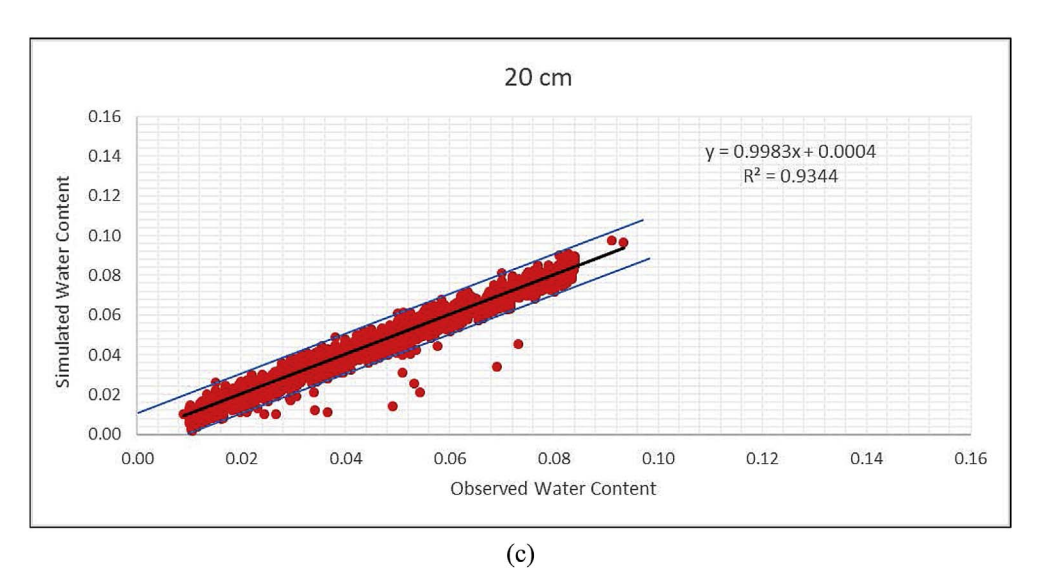
c Relative root mean square error (Equation (6)).





(a)





automatically stored by a data logger at a same time interval of 10 min. The sensors for the weather station are Model L3 of Yangguang Co. Ltd. (http://jz322.shuoyi.com): the precipitation sensor has an accuracy of \pm 0.1 mm, the temperature sensor has an accuracy of \pm 0.1 °C, and the other sensors have an accuracy of \pm 0.5%. The sensors for soil moisture are CNC503-B, made by Qudao Co. Ltd. (http://www.chem17.

com) with an accuracy of \pm 0.4%, while the sensors for soil temperature are LVDWZ-31, made by Xinlvyuan Co. Ltd. (http://www.caigou.com.cn) with an accuracy of \pm 0.1° C. The TNHP sensor for surface soil temperature and water content is RM-003, made by Ruiming Com. (http://www.czruiming.com) with an accuracy of \pm 0.1 °C and \pm 0.4%, respectively. The details of the sensors and their installation can

S. Pedram et al.

Table 4 Performance measures of the HYDRUS-1D model for the validation period (Jan. 1 to Dec. 31, 2014). $^{\rm a}$

Depth below the Ground Surface (cm)	Soil Tempe	erature				Soil Water	Content			
	Mean (°C)	Std. (°C)	Cv^{b}	RRSME ^c	R2	Mean	Std.	Cv ^b	RRSME ^c	R2
5	4.33 (4.77)	3.17 (3.21)	0.73 (0.65)	0.124	0.92	0.011 (0.013)	0.0014 (0.0015)	0.13 (0.11)	0.222	0.76
10	5.63 (6.56)	2.12 (2.44)	0.37 (0.37)	0.147	0.84	0.029 (0.026)	0.0013 (0.0011)	0.044 (0.042)	0.205	0.78
20	7.48 (8.99)	2.08 (2.87)	0.27 (0.3')	0.199	0.78	0.059 (0.069)	0.0011 (0.0013)	0.018 (0.018)	0.187	0.80
30	8.12 (9.87)	3.05 (3.16)	0.37 (0.32)	0.215	0.75	0.066 (0.071)	0.0019 (0.0018)	0.028 (0.025)	0.176	0.92
40	9.57 (10.11)	3.14 (3.18)	0.32 (0.31)	0.183	0.80	0.084 (0.096)	0.0021 (0.0027)	0.025 (0.028)	0.172	0.93
50	10.11 (11.22)	1.22 (1.67)	0.12 (0.14)	0.117	0.93	0.106 (0.115)	0.0031 (0.004)	0.029 (0.034)	0.153	0.98

 $^{^{\}rm a}$ The value in bracket is the measured.

^c Relative root mean square error (Equation (6)).

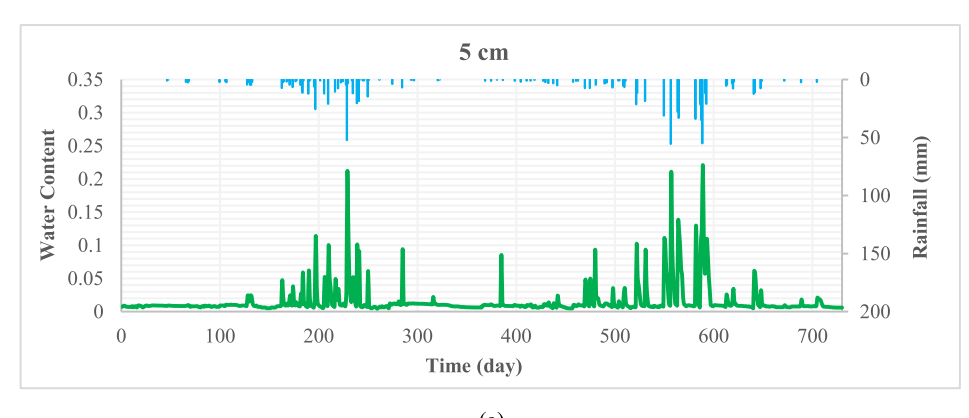
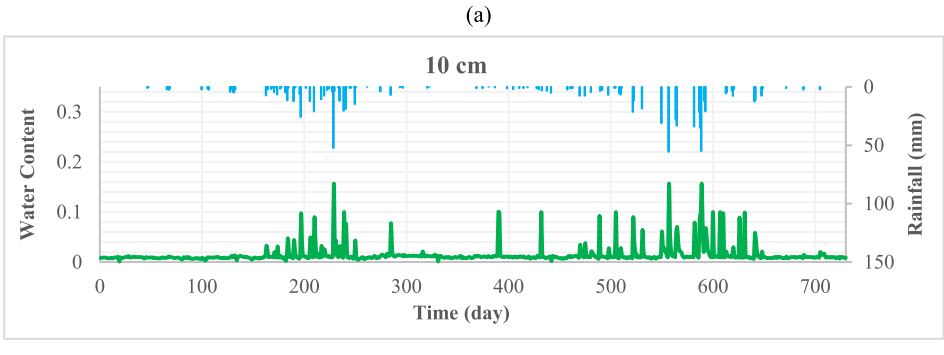
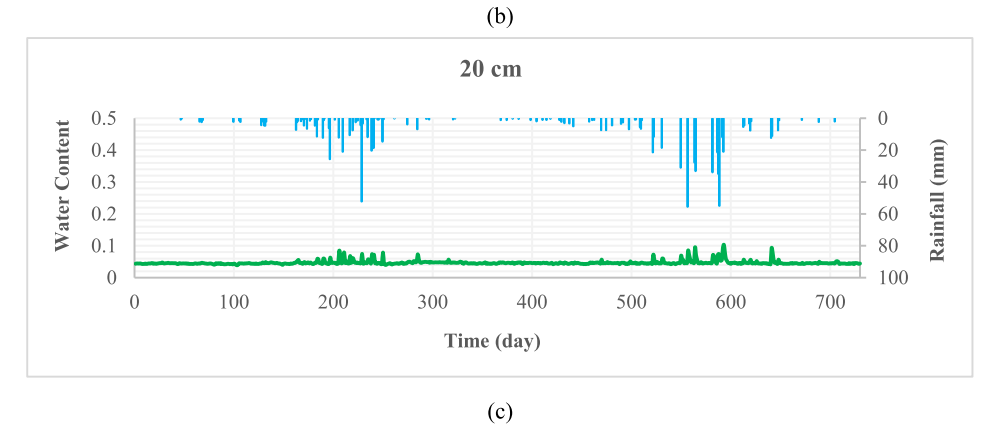


Fig. 6. Diurnal variations of water content in three different soil layers for the two simulation years.





^b Coefficient of variation, defined as the ratio of standard deviation (Std.) to mean.

Means and standard deviations (in brackets) of the pore air relative humidity within different soil layers for year 2013.

	Days	Pore Air Relativ	Pore Air Relative Humidity (RH_{pa}) in Year 2013	$_{\rm pa}$) in Year 2013										
гауег		Annual	Jan	Feb	Mar	Apr	May	Jun	Jul	Aug	Sep	Oct	Nov	Dec
Surface I	Ory	45.57 (8.66)	57.73 (9.66)	56.66 (7.76)	52.28 (8.33)	50.12 (6.78)	48.23 (7.12)	41.22 (7.55)	40.12 (9.22)	38.22 (10.11)	39.45 (9.87)	41.12 (10.12)	54.43 (10.43)	56.66 (9.44)
_	Wet	79.66 (15.77)	80.12 (19.11)	78.89 (16.78)	72.55 (15.44)	79.43 (13.24)	75.54 (11.31)	72.22 (22.20)	69.87 (18.81)	71.12 (17.72)	67.56 (15.55)	78.65 (18.81)	79.12 (17.71)	76.12 (19.71)
0-5 Cm I	Dry	65.67 (7.46)	69.66 (7.44)	63.22 (6.54)	71.22 (7.45)	56.87 (7.77)	61.22 (6.45)	63.22 (7.12)	65.54 (8.22)	71.22 (9.22)	66.65 (7.78)	61.34 (10.09)	69.13 (9.88)	78.83 (9.18)
_	Wet	84.34 (13.65)	88.12 (14.44)	89.34 (14.33)	82.22 (14.34)	81.33 (12.33)	79.42 (10.11)	69.99 (11.12)	71.12 (14.41)	82.14 (16.66)	85.44 (15.66)	81.22 (16.66)	78.23 (15.24)	81.27 (17.24)
5-10 cm I	Dry	77.34 (5.22)	79.12 (6.66)	78.88 (5.24)	74.22 (6.66)	66.87 (5.34)	66.75 (6.12)	69.12 (6.12)	69.23 (7.22)	78.88 (8.89)	72.29 (7.76)	73.33 (9.99)	74.48 (9.99)	79.90 (9.12)
_	Wet	88.66 (12.56)	89.32 (12.37)	85.66 (11.33)	86.44 (12.22)	83.45 (10.44)	83.23 (9.12)	79.92 (10.21)	79.45 (12.29)	84.56 (13.33)	84.44 (10.81)	84.44 (12.11)	84.22 (14.41)	85.66 (13.91)
10-20 cm I	Dry	79.34 (4.33)	81.21 (5.45)	83.33 (6.05)	79.56 (5.44)	75.22 (5.12)	71.23 (7.23)	72.22 (7.22)	73.23 (6.66)	80.21 (7.21)	83.33 (6.89)	78.88 (7.12)	81.12 (8.81)	82.78 (7.78)
_	Wet	89.45 (11.12)	88.32 (12.88)	89.22 (13.33)	84.34 (11.23)	87.33 (9.22)	82.76 (8.33)	86.12 (10.12)	78.88 (10.12)	83.33 (11.22)	89.43 (10.32)	86.66 (9.18)	89.22 (13.39)	88.89 (11.28)
20-30 cm I	Dry	80.12 (4.12)	82.23 (4.87)	83.29 (5.98)	80.22 (5.23)	79.23 (4.21)	75.22 (6.12)	74.44 (6.22)	77.98 (6.23)	83.43 (6.23)	86.65 (5.59)	81.12 (6.21)	84.44 (7.79)	85.15 (7.12)
	Wet	90.13 (9.55)	89.99 (12.67)	90.09 (11.18)	88.33 (11.12)	83.46 (10.12)	81.14 (8.88)	79.87 (9.32)	81.67 (9.99)	89.22 (9.99)	(86.6) 60.06	87.77 (7.18)	89.99 (11.12)	90.12 (10.11)
30-40 cm I	Dry	82.32 (3.22)	89.44 (4.44)	87.71 (4.44)	85.55 (4.32)	83.52 (3.12)	79.33 (5.87)	82.21 (5.22)	82.22 (6.12)	85.22 (5.12)	88.88 (5.21)	84.44 (5.22)	87.71 (6.61)	88.32 (6.69)
_	Wet	(89.89)	90.23 (11.44)	91.12 (13.22)	90.21 (10.09)	89.56 (9.55)	84.45 (9.12)	89.32 (8.88)	88.21 (8.88)	90.12 (8.32)	92.23 (8.71)	87.77 (6.23)	91.11 (10.92)	91.23 (9.34)
40-50 cm	Dry	85.12 (3.12)	89.64 (3.22)	88.22 (4.09)	87.54 (2.12)	89.91 (2.29)	84.23 (4.12)	86.66 (4.10)	85.55 (5.44)	87.33 (5.22)	89.19 (4.43)	88.32 (3.78)	89.34 (5.54)	90.12 (5.13)
_	Wet	90.08 (7.99)	90.33 (9.98)	91.12 (10.44)	90.23 (9.23)	91.12 (8.78)	89.19 (8.33)	87.34 (7.74)	89.92 (7.33)	90.21 (7.21)	94.43 (7.77)	93.68 (5.78)	92.22 (9.43)	91.99 (8.12)
50-60 cm	Dry	86.32 (2.11)	90.05 (2.54)	89.32 (3.33)	88.22 (2.09)	90.12 (2.45)	87.12 (3.22)	87.77 (3.21)	90.1	88.87 (4.42)	91.11 (3.12)	90.21 (2.21)	90.22 (4.12)	91.12 (3.38)
	Wet	90.33 (6.67)	90.34 (6.55)	92.44 (9.16)	91.11 (8.65)	96.32 (6.34)	92.12 (7.77)	90.12 (8.61)	(3.12) 91.21 (6.66)	92.22 (7.73)	93.33 (8.22)	98.45 (5.45)	91.23 (6.34)	92.12 (7.34)
														Ī

be found in Duan et al. (2011, 2015).

In this study, the data from 1 January 2013 to 31 December 2014 were used. The data for the first year (2013) were used to calibrate the HYDRUS-1D model, while the data for the second year (2014) were used to validate the model. Subsequently, the simulated results for both years were used to examine the dynamics of SWC and $\mathrm{RH}_{\mathrm{pa}}$. The annual precipitation in 2013 was smaller than the average annual precipitation (344.9 versus 389 mm), whereas, the annual precipitation in 2014 was larger than the average annual precipitation (520.6 versus 389 mm) (Table 1). This indicates that year 2013 was relatively drier while year 2014 was relatively wetter. However, both years shared a similar temporal variation pattern in seasonal precipitation, with wettest months of June, July, and August. For these three wettest months, there were fewer rainy days but higher rainfall intensities in 2014 than 2013, while for the other months, there were more rainy days and higher rainfall intensities in 2014 than 2013 (Fig. 3). Overall, regardless of the years, more than 85% of the days had no precipitation and could be subject to net losses of soil water.

2.4. Model set up

The model was set up for a 120-cm-deep soil profile with a uniform spatial discretization of 1 cm, leading to 120 layers (121 nodes) for mass balances. The sensors at 0, 10, 20, 40, 80, and 120 cm depths are six of the 121 nodes (hereinafter designated as "sensor nodes" for description purposes). For each layer, its preliminary soil-water parameters (Table 2) were determined using laboratory experiments conducted by the authors (Duan et al., 2011) as well as from literature (Ghanbarian-Alavijeh et al., 2010). Herein, the soil water retention function was defined by the van Genuchten (1980) equation. In addition, for each sensor node, the initial condition was specified as the measured value at 0:10 January 1, 2013, while for a non-sensor node, the initial condition was determined to be the linear interpolation of the measured values at the two adjacent sensor nodes. For instance, the initial condition at the 1-cm-depth node was determined to be $0.9\theta_{0.0}$ + 0.10_{10.0}, and the initial condition at the 18-cm-depth node was determined to be $0.2\theta_{10,0} + 0.8\theta_{20,0}$, where $\theta_{0,0}$, $\theta_{10,0}$, and $\theta_{20,0}$ are the initial water contents at surface, 10-cm-depth, and 20-cm-depth nodes, respectively. Further, the upper boundary conditions were defined as the time series of precipitation, surface soil temperature, and E_s (potential evapotranspiration). Es was estimated by the Penman-Monteith method (Monteith, 1965; Wang et al., 2006) using the measured data on air temperature, atmosphere relative humidity, solar radiation, and wind speed. Moreover, the lower boundary condition was specified to be free drainage because of the deep (> 4 m) water table, as mentioned above.

The model was run from 1 January 2013 to 31 December 2014, with a computational time step of 10 min. The model was calibrated using the data on SWC and soil temperature for 2013 and then validated using the responding data for 2014. The calibration was implemented by manually adjusting the parameters listed in Table 2 to make the simulated soil temperatures and water contents closely match the responding measured values, as indicated by the model performance measures to be described in the following context (i.e., section 2.5). These parameters were selected because previous studies (e.g., Šejna et al., 2011; Šimůnek et al., 2011) indicated that they are sensitive for HYDRUS-1D simulations. Given that α and n, two parameters of the van Genuchten (1980) equation, could not be directly measured and thus might be relatively uncertain, they were first adjusted one at a time. Subsequently, the three soil-water parameters, Q_r (residual soil water content), Q_s (saturated soil water content), and K_s (saturated hydraulic conductivity), were adjusted in this order one at a time. Finally, the tortuosity parameter, I, in the conductivity function was adjusted. At the beginning, each of these parameters was assigned to be the mean of its range given in Table 2. That is, the beginning values were $\alpha = 0.365 \text{ cm}^{-1}$, n = 4.475, $Q_r = 0.05$, $Q_s = 0.40$, and

Table 5b

Means and standard deviations (in brackets) of the pore air relative humidity within different soil layers for year 2014.

Soil Layer	Days	Pore Air I	Relative Hun	nidity (RH _{pa})	in Year 201	4								
Layer		Annual	Jan	Feb	Mar	Apr	May	Jun	Jul	Aug	Sep	Oct	Nov	Dec
Surface	Dry	48.88	54.46	56.66	55.34	51.12	35.55	40.77	75.12	73.22	70.13	78.12	71.48	38.66
		(8.66)	(11.61)	(7.76)	(10.45)	(11.21)	(8.69)	(12.34)	(10.11)	(11.65)	(9.99)	(11.12)	(11.43)	(10.44)
	Wet	79.66	78.66	78.89	68.56	55.22	59.99	52.23	75.12	75.44	76.54	81.65	75.12	44.12
		(15.77)	(17.57)	(16.78)	(13.23)	(16.78)	(10.78)	(16.67)	(14.44)	(17.72)	(13.23)	(15.81)	(12.71)	(15.71)
0-5 cm	Dry	65.67	71.32	63.22	69.34	61.47	45.87	55.34	81.23	78.23	71.65	84.34	79.13	44.13
		(7.46)	(4.44)	(6.54)	(5.34)	(6.66)	(5.23)	(4.23)	(5.23)	(4.12)	(5.78)	(6.09)	(6.83)	(5.18)
	Wet	84.34	78.33	89.34	72.22	70.33	51.39	60.12	86	81.12	76.44	85.22	81.23	52.27
		(13.65)	(11.22)	(14.33)	(9.34)	(14.44)	(8.76)	(5.67)	(10.12)	(9.23)	(11.66)	(12.66)	(10.24)	(13.24)
5-10 cm	Dry	77.34	79.12	78.88	72.33	66.87	48.67	70.32	83.23	88.23	83.29	85.93	80.43	46.90
		(5.22)	(4.11)	(5.24)	(5.01)	(5.34)	(5.23)	(4.12)	(5.12)	(3.08)	(4.76)	(5.69)	(5.99)	(4.12)
	Wet	88.66	83.32	85.66	78.45	71.12	51.09	75.24	85.33	89.09	86.44	88.44	85.23	56.66
		(12.56)	(10.37)	(11.33)	(8.12)	(9.99)	(6.57)	(5.23)	(8.23)	(6.12)	(8.87)	(9.11)	(9.12)	(10.91)
10-20 cm	Dry	79.34	80.33	80.11	85.44	78.89	52.76	80.13	84.44	89.87	85.65	88.12	82.12	48.71
		(4.33)	(4.01)	(5.09)	(4.65)	(4.44)	(4.23)	(3.43)	(4.23)	(3.04)	(4.34)	(5.12)	(4.81)	(3.12)
	Wet	89.45	88.32	86.32	88.91	81.66	60.12	82.22	87.43	90.12	88.43	86.66	84.28	55.77
		(11.12)	(9.77)	(8.49)	(7.23)	(8.78)	(8.33)	(4.23)	(7.32)	(5.19)	(9.98)	(8.18)	(8.35)	(8.13)
20-30 cm	Dry	80.12	82.22	82.21	88.23	81.21	50.21	85.22	86.34	90.22	87.65	89.32	85.22	55.11
	-	(4.12)	(3.32)	(4.44)	(4.12)	(3.33)	(3.33)	(2.32)	(4.12)	(2.23)	(3.59)	(4.11)	(3.22)	(3.11)
	Wet	90.13	87.99	87.19	90.12	84.56	61.11	87.21	88.34	91.23	91.79	90.77	88.99	60.12
		(9.55)	(6.76)	(7.45)	(7.09)	(7.99)	(6.23)	(3.39)	(6.21)	(4.44)	(6.98)	(6.18)	(7.08)	(7.06)
30-40 cm	Dry	82.32	88.55	83.33	85.55	85.34	52.11	89.76	87.12	91.11	89.48	90.41	88.71	58.38
	-	(3.22)	(3.08)	(3.34)	(4.32)	(3.09)	(2.22)	(1.21)	(3.21)	(2.09)	(3.21)	(4.09)	(3.61)	(2.69)
	Wet	89.89	89.99	89.76	91.13	86.77	68.12	90.12	88.21	91.32	93.23	91.77	93.09	65.23
		(8.67)	(5.23)	(6.32)	(6.87)	(6.54)	(5.12)	(3.32)	(5.21)	(4.12)	(5.71)	(5.23)	(6.92)	(8.34)
40-50 cm	Dry	85.12	90.44	85.55	90.09	86.66	55.65	92.12	89.11	92.22	89.99	92.32	90.32	59.12
	,	(3.12)	(2.24)	(3.12	(2.89)	(2.12)	(2.34)	(1.09)	(3.11)	(1.98)	(3.13)	(3.18)	(3.14)	(2.13)
	Wet	90.08	93.33	90.22	91.12	92.22	67.32	93.3	90.76	93.21	92.43	93.55	92.56	61.99
		(7.99)	(4.45)	(5.12)	(5.34)	(5.34)	(4.12)	(2.12)	(4.22)	(3.21)	(4.77)	(4.78)	(5.49)	(5.12)
50-60 cm	Dry	86.32	91.55	91.21	92.12	91.21	59.11	94.44	90.59	93.87	90.11	95.21	92.45	61.77
	-	(2.11)	(2.32)	(2.23)	(1.09)	(1.78)	(1.99	(1.02)	(2.25)	(1.42)	(2.12)	(2.21)	(2.56)	(2.09)
	Wet	90.33	93.37	94.11	92.89	94.34	69.32	95.22	92.24	94.22	91.12	98.45	93.13	65.33
		(6.67)	(4.12)	(5.09)	(4.44)	(4.32)	(3.33)	(2.09)	(4.12)	(2.73)	(4.22)	(4.45)	(4.34)	(4.99)

 $\rm K_s=860~cm~d^{-1}$, and I = 0.65. When one parameter was adjusted, the values for the other parameters were kept unchanged. The adjustment was tried by both increasing and decreasing the parameter value by an empirical delta. The adopted value for this parameter was the one at which the model performed best in terms of the measures to be discussed in section 2.5. This adopted value was kept unchanged when another parameter was adjusted.

2.5. Measures of model performance

In addition to visualization plots showing the simulated versus measured time series of soil temperatures and water contents, two commonly-used statistics, namely coefficient of determination (R^2) and coefficient of variation $(C_{\rm v}),$ were also computed. R^2 measures the percentage of the variations presented in a measured time series that can be explained by the model, whereas, $C_{\rm v}$ measures the spread (i.e., amount of variability) in relative to the mean of the time series. A good model is expected to have a relatively large R^2 value and give a $C_{\rm v}$ value close to that of the responding measured time series. Further, the relative (i.e., normalized) root mean square error, RRSME, was also computed and used to measure the model performance. RRSME can be computed as:

$$RRSME = \frac{\sqrt{\frac{\sum_{i=1}^{N}(M_{i} - C_{i})^{2}}{N}}}{Max(M_{1}, M_{2}, ..., M_{N}) - Min(M_{1}, M_{2}, ..., M_{N})}$$
(6)

where N is the number of times; M_i is the measurement at ith time; C_i is the simulated value at ith time; Max () is the maximum function; and Min() is the minimum function.

RRSME can vary from zero to $+\infty$. A zero value indicates that the model can perfectly reproduce the measurements, whereas, a greater positive value indicates a poorer model performance. In relation with

the symbols in Equations (1)–(5), when RRSME was computed for SWC, $M_{\rm i}$ and $C_{\rm i}$ are the measured and simulated values for θ at ith time, respectively, when RRSME was computed for soil temperature, on the other hand, $M_{\rm i}$ and $C_{\rm i}$ are the measured and simulated values for T at ith time, respectively.

2.6. Examination of the simulated SWC and RH_{pa} dynamics

For each simulation year, at the annual or monthly time scale, the means and standard deviations of the simulated time series of SWC and RH_{pa} were computed for eight soil layers, including the surface, 0–5 cm (Layer 1), 5–10 cm (Layer 2), 10–20 cm (Layer 3), 20–30 cm (Layer 4), 30–40 cm (Layer 5), 40–50 cm (Layer 6), and 50–60 cm (Layer 7).

The computations were done for the dry (i.e., non-rainy) and wet (i.e., rainy) days, respectively. The computed means and standard deviations were compared to examine relative magnitudes and vertical distributions of the simulated values for SWC and $RH_{\rm pa}.$ In addition, the diurnal variations of the SWC and $RH_{\rm pa}$ were scrutinized by plotting the simulated values for selected dry and wet days. Herein, because it is still an unresolved scientific challenge to accurately measure $RH_{\rm pa}$ in sandy soils (Goss and Madliger, 2007), this study could not use data on $RH_{\rm pa}$ to calibrate/validate the HYDRUS-1D model. However, it was empirically judged that the simulated values of $RH_{\rm pa}$ were probably more appropriate for assessing the relative diurnal variations of pore vapor, which is the focus of this study, rather than determining the absolute magnitudes of $RH_{\rm pa}.$

3. Results

3.1. The calibrated HYDRUS-1D model

The adopted model parameters are presented in Table 2. During the

S. Pedram et al.

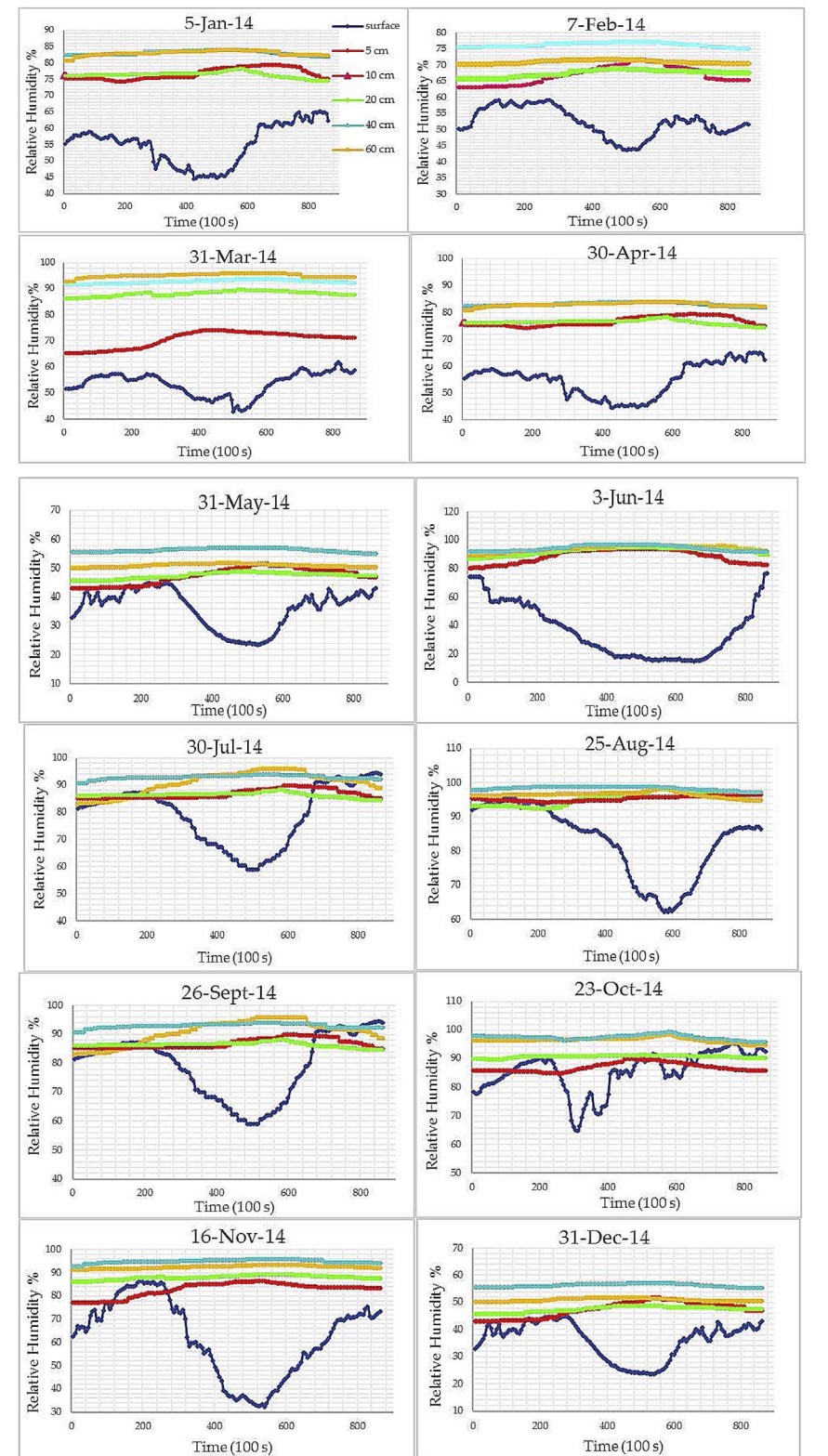


Fig. 7. The simulated diurnal variations of pore air relative humidity $(RH_{\rm pa})$ within the soil layers for the selected dry (i.e., nonrainy) days.

calibration period (January 1 to December 31, 2013), the model well reproduced the soil temperatures measured at the 5, 10, and 20 cm depths below the ground surface, as indicated by $\rm R^2>0.79$ and that few of the values fall out of the 95% confidence limits of the simulated-measured regression lines (Fig. 4). For a given soil layer, the model tended to underestimate the mean of the measured soil temperatures by about 0.96 °C, whereas, it tended to overestimate the temporal variation in the measured soil temperatures, as indicated by the larger

coefficient of variation (C_v) for the simulated soil temperatures than that for the measured soil temperatures (Table 3). The model had a similar performance for all soil layers, as indicated by the similar values of RRSME or R^2 between the layers. On the other hand, the model also well reproduced the soil water contents measured at the same depths, as indicated by $R^2 > 0.78$ and that few of the values fall out of the 95% confidence limits of the simulated-observed regression lines (Fig. 5). Overall, the model performed slightly better in simulating the soil water

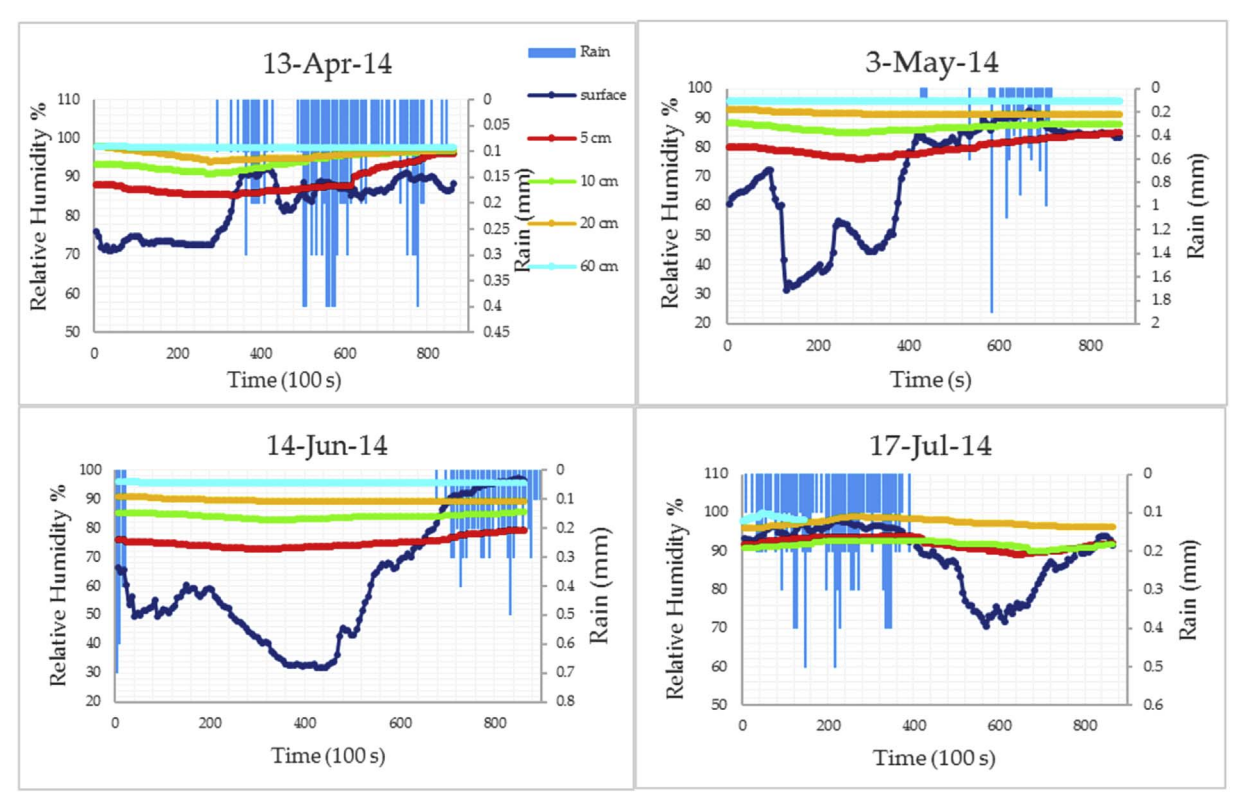


Fig. 8. The simulated diurnal variations of pore air relative humidity (RH_{pa}) within the soil layers for the selected wet (i.e., rainy) days.

contents than the soil temperatures. For a given soil layer, the model tended to underestimate the mean of the observed soil water contents by 22%, while it also tended to underestimate the temporal variation of the observed soil water contents, as indicated by the smaller $C_{\rm v}$ for the simulated soil water contents than that for the measured soil water contents (Table 3). Again, the model had a similar performance for all soil layers in reproducing the measured soil water contents.

During the validation period (January 1 to December 31, 2014), the model also did a good job ($R^2 \geq 0.75$; RRSME ≤ 0.215) (Table 4). The similar performance for both periods indicates that the model is very robust and can be applicable for different climatic and/or soil-water conditions. Hence, the calibrated model was judged to be accurate enough to mimic the physical processes of the two-phase fluids (i.e., water vapor and liquid water) for the study site, which is the focus of this study.

Fig. 6 shows the variation of the simulated water content in the 5, 10, and 20 cm layers for 2013 and 2014. Regardless of the layers, during the dry months with a minimal amount of precipitation, the water content was predicted to be very low, whereas, during the wet (i.e., summer) months with a high-intensity precipitation, the water content was predicted to be relatively high but to decline very quickly once rain stopped. The reason for the quick decline can be attributed to the high rate of evaporation, which might reach to 178.5 mm d $^{-1}$ in summer.

3.2. The simulated pore air relative humidity

At the annual and monthly time scales, regardless of dry or wet days, the average pore air relative humidity (RH $_{\rm pa}$) increased with soil depth (Tables 5a and 5b). The increasing gradient within the top 10 cm layer was much larger than that within a lower soil layer, in particularly for the dry days. As expected, for a given time scale, the average RH $_{\rm pa}$ of a dry day was smaller than that of a wet day. However, the RH $_{\rm pa}$ within an upper soil layer had a greater temporal variation (i.e., standard deviation) than that within a lower soil layer. That is, the RH $_{\rm pa}$ within

an upper soil layer varied more greatly from time to time.

For a given dry (i.e., non-rainy) day, the RH_{pa} within the surface layer had a much greater temporal variation than that within a deeper layer (Fig. 7). Overall, the RH_{pa} within the surface layer reached its minimum around 14:00 (i.e., 50,000 s in the figure), while the RH_{pa} within the 5- or 10-cm layer approached its maximum around this same time. The RH_{pa} within the layers below the depth of 10 cm was almost constant throughout the day. At a given time during the day, the RH_{pa} within a deeper layer tended to be larger than that within a shallower layer.

In contrast, for a wet (i.e., rainy) day, the RH_{pa} within the surface layer could be larger than that within a deeper layer, and the timing of its minimum was dependent of the timing and amount of rainfall (Fig. 8). When rain fell either in the morning or afternoon, the RH_{pa} within the surface layer occurred around 14:00. The RH_{pa} within a layer below the surface was almost constant throughout the day regardless of the rain pattern. The RH_{pa} within a deeper layer tended to be larger than that within a shallower layer, which is consistent with that for a dry day.

3.3. The simulated water content

At the annual and monthly time scales, regardless of dry or wet days, the average volumetric water content of nonrainy days increased with soil depth (Tables 6a and 6b). The increasing gradient within the top 10 cm was generally smaller than that within a lower soil depth, in particularly for the dry days. As expected, for a given time scale, the average water content of a dry day was smaller than that of a wet day. However, the water content within an upper soil layer had a greater temporal variation (i.e., standard deviation) than that within a lower soil layer. That is, the water content within an upper soil layer varied more greatly from time to time. For a given dry day, the water content within the surface layer had a much greater temporal variation than that within a deeper layer (Fig. 9). Overall, the water content within the surface layer reached its minimum around 14:00 (i.e., 50,000 s in the

Table 6a
Means and standard deviations (in brackets) of the volumetric water contents within different soil layers for year 2013.

).0092 (0.00012) -	0.0098 (0.0001) -	0.0112 (0.00089) -	0.0133 (0.0007) - 0.0201	(0.0008) - 0.0251 (0.00065)	0.0322 (0.00055) -
Dec	0.0	0.0	0.0	0.0).0) 1 0:00 1	0.0
Nov	0.0093 (0.00013) 0.0154 (0.0015)	(0.00010) (0.00010) (0.00666 (0.00143)	0.0136 (0.00093) 0.0388 (0.00129)	0.0144 (0.00088) 0.0332 (0.00121) 0.0266	(0.00082) 0.0344 (0.00119) 0.0278 (0.00081) 0.0312	(0.00079) 0.0385 (0.00079) 0.0395 (0.00099)
Oct	0.0117 (0.00087) 0.0932 (0.00142)	(0.00062) (0.09062) (0.00133)	0.0153 (0.00051) 0.0612 (0.00119)	0.0162 (0.00059) 0.0603 (0.00191)	(0.00055) 0.0566 (0.00188) 0.0266 (0.00054) 0.0412	(0.00177) 0.0459 (0.00051) 0.0499 (0.00171)
Sep	0.0111 (0.00011) 0.0850 (0.00032)	(0.0011) (0.0001) (0.0801) (0.00142)	0.0155 (0.00107) 0.0701 (0.00133)	0.0167 (0.00104) 0.0693 (0.00129) 0.0255	(0.00099) 0.0555 (0.00111) 0.0367 (0.000910 0.0523	0.0479 (0.00088) 0.0484 (0.00104)
Aug	0.0132 (0.00098) 0.210 (0.00166)	(0.00083) (0.00083) (0.00142)	0.0191 (0.00094) 0.0860 (0.00062)	0.0193 (0.00089) 0.0763 (0.00169) 0.0241	(0.00082) 0.0688 (0.00079) 0.0455 (0.00075) 0.0623	
Jul	0.0123 (0.00016) 0.114 (0.00106)	0.0139 (0.0007)	0.0181 (0.00045) 0.0823 (0.000978)	0.0196 (0.00034) 0.0755 (0.00072) 0.0271	(0.00079) 0.0689 (0.00169) 0.0413 (0.00071) 0.0532	0.00143)
Jun	0.0108 (0.0009) 0.0855 (0.0011)	0.0121 (0.00044) 0.0766 (0.0009)	0.0176 (0.00033) 0.0612 (0.00049)	0.0186 (0.00081) 0.0557 (0.00193) 0.0254	(0.00079) 0.0598 (0.00077) 0.0366 (0.00066) 0.0514	(0.00055) (0.00055) (0.00493
May	0.0101 (0.0001) 0.0275 (0.0007)	(0.00019) (0.00019) (0.0065)	0.0162 (0.00012) 0.0259 (0.00144)	0.0171 (0.00010) 0.0232 (0.00141) 0.0253	(0.00088) 0.0312 (0.00139) 0.0322 (0.00081) 0.0478	(0.0077) (0.0484 (0.0484 (0.00109)
Apr	0.0082 (0.00023) 0.0241 (0.00044)	(0.00012) (0.00012) (0.0223 (0.00037)	0.0118 (0.00010) 0.0201 (0.00019)	0.0121 (0.00093) 0.0199 (0.00157)	(0.00088) 0.0312 (0.00144) 0.0301 (0.00079) 0.0433	(0.0011) (0.00065) (0.0488 (0.00111)
Mar	0.0071 (0.0005) 0.0198 (0.0002)	(0.00042) (0.00042) (0.00018)	0.0121 (0.00126) 0.0182 (0.00178)	0.0123 (0.00119) 0.0166 (0.00169)	(0.00111) 0.0201 (0.00158) 0.0293 (0.00105) 0.0391	(0.00132) (0.00132)
Feb	0.0058 (0.0001) 0.0132 (0.001)	(0.0052) (0.00086) (0.0114 (0.00042)	0.0091 (0.00054) 0.0131 (0.000212)	0.0108 (0.00049) 0.0127 (0.00208) 0.0166	(0.00138) 0.0288 (0.00199) 0.0283 (0.00129) 0.0312	(0.00123) 0.0442 (0.00177)
Jan	0.0041 (0.0002)	0.0062 (0.0003)	0.0099 (0.00019)		(0.00012) - 0.0208 (0.00014)	0.0360 (0.00012) -
Annual	0.0085 (0.00065) 0.0687 (0.0012)	(0.0006) (0.0459 (0.00088)	0.0131 (0.00055) 0.0476 (0.00112)	0.0141 (0.0009) 0.0439 (0.0012) 0.0194	(0.0008) 0.0455 (0.0012) 0.0293 (0.00112) 0.0453	(0.0005) (0.00065) (0.0015)
Days	Dry Wet	Dry Wet	Dry Wet	Dry Wet Dry	Wet Dry Wet	Dry Wet
Soil Layer Days Annual	Surface	0–5 cm	10–20 cm	20-30 cm 30-40 cm	40–50 cm	50–60 cm

Table 6b

Means and standard deviations (in brackets) of the volumetric water contents within different soil layers for year 2014.

Soil Layer	Days	Annual	Jan	Feb	Mar	Apr	May	Jun	Jul	Aug	Sep	Oct	Nov	Dec
Surface	Dry	0.0131	0.0055	0.0069	0.0086	0.0099	0.0128	0.0142	0.0153	0.0177	0.0166	0.0133	0.0129	0.0107
		(0.0012)	(0.00098)	(0.00132)	(0.00122)	(0.00115)	(0.00145)	(0.00138)	(0.00128)	(0.00144)	(0.00173)	(0.00168)	(0.00173)	(0.00166)
	Wet	0.0598	0.0116	0.0144	0.0182	0.0232	0.0298	0.101	0.121	0.231	0.0544	0.0596	0.0229	0.0218
		(0.0018)	(0.00197)	(0.00166)	(0.00110)	(0.00197)	(0.00197)	(0.00166)	(0.00156)	(0.00194)	(0.00188)	(0.00230)	(0.00188)	(0.00178)
0–5 cm	Dry	0.015	0.0076	0.0081	0.0104	0.0128	0.0155	0.0245	0.0257	0.0182	0.0169	0.0154	0.0134	0.0122
		(0.0012)	(0.00154)	(0.00129)	(0.00119)	(0.00104)	(0.00132)	(0.00132)	(0.00122)	(0.00141)	(0.00161)	(0.00155)	(0.00166)	(0.00161)
	Wet	0.0536	0.0148	0.0166	0.0199	0.0244	0.0223	0.0956	0.104	0.203	0.0507	0.0443	0.0266	0.0210
		(0.00182)	(0.00187)	(0.00159)	(0.00208)	(0.00181)	(0.00192)	(0.00162)	(0.00153)	(0.00188)	(0.00185)	(0.00226)	(0.00182)	(0.00170)
5–10 cm	Dry	0.0134	0.0105	0.0116	0.0118	0.0133	0.0162	0.0257	0.0268	0.0202	0.0175	0.0167	0.0148	0.0134
		(0.0011)	(0.00142)	(0.00122)	(0.00098)	(0.00102)	(0.00124)	(0.00122)	(0.00119)	(0.00139)	(0.00155)	(0.00149)	(0.00161)	(0.00159)
	Wet	0.0482	0.0143	0.0161	0.0195	0.0232	0.0218	0.0907	0.0998	0.1552	0.0492	0.0434	0.0255	0.0203
		(0.0015)	(0.00172)	(0.00132)	(0.00197)	(0.00198)	(0.00188)	(0.00157)	(0.00144)	(0.00182)	(0.00179)	(0.00219)	(0.00179)	(0.00159)
10-20 cm	Dry	0.0193	0.0163	0.0177	0.0181	0.0188	0.0194	0.0284	0.0284	0.0224	0.0202	0.0184	0.0155	0.0129
		(0.0012)	(0.00134)	(0.00119)	(0.00091)	(0.00099)	(0.00118)	(0.00115)	(0.00097)	(0.00112)	(0.00143)	(0.00144)	(0.00155)	(0.00146)
	Wet	0.0427	0.0205	0.0222	0.0252	0.0277	0.0208	0.0823	0.0898	0.0999	0.0402	0.0412	0.0233	0.0202
		(0.0015)	(0.00166)	(0.00125)	(0.00188)	(0.00181)	(0.00172)	(0.00142)	(0.00132)	(0.00175)	(0.00171)	(0.00198)	(0.00165)	(0.00138)
20-30 cm	Dry	0.0212	0.0173	0.0182	0.0198	0.0198	0.0202	0.0295	0.0296	0.0252	0.0223	0.0217	0.0164	0.0155
		(0.0011)	(0.00129)	(0.00106)	(0.00089)	(0.00091)	(0.00107)	(0.00104)	(0.00088)	(0.00102)	(0.00121)	(0.00138)	(0.00143)	(0.00142)
	Wet	0.0395	0.0203	0.0205	0.0233	0.0266	0.0209	0.0817	0.0743	0.0823	0.0397	0.0393	0.0226	0.0200
		(0.0013)	(0.00162)	(0.00112)	(0.00175)	(0.00176)	(0.00166)	(0.00134)	(0.00121)	(0.00162)	(0.00165)	(0.00187)	(0.00154)	(0.00122)
30-40 cm	Dry	0.024	0.0204	0.0208	0.0219	0.0239	0.0232	0.0301	0.0332	0.0304	0.0244	0.0267	0.0184	0.0161
		(0.0009)	(0.00112)	(0.00098)	(0.00082)	(0.00087)	(0.00095)	(0.00095)	(0.00076)	(0.00123)	(0.00109)	(0.00124)	(0.00132)	(0.00139)
	Wet	0.0558	0.0245	0.0229	0.224	0.0255	0.0254	0.0801	0.0681	0.0788	0.0429	0.0387	0.0211	0.0185
		(0.0012)	(0.00154)	(0.00101)	(0.00166)	(0.00152)	(0.00161)	(0.00121)	(0.00115)	(0.00157)	(0.00155)	(0.00165)	(0.00144)	(0.00105)
40-50 cm	Dry	0.0323	0.0223	0.0294	0.0237	0.0284	0.0292	0.0452	0.0499	0.0453	0.0323	0.0366	0.0245	0.0212
	-	(0.0006)	(0.00098)	(0.00087)	(0.00076)	(0.00077)	(0.00083)	(0.0078)	(0.00069)	(0.00115)	(0.00088)	(0.00133)	(0.00129)	(0.00122)
	Wet	0.0439	0.0387	0.0298	0.0316	0.0381	0.0344	0.0754	0.0632	0.062	0.0402	0.0432	0.0386	0.0275
		(0.0012)	(0.00134)	(0.00096)	(0.00146)	(0.00134)	(0.00155)	(0.00119)	(0.00104)	(0.00108)	(0.00149)	(0.00144)	(0.00139)	(0.00116)

figure), whereas, the water content within a deeper layer was almost constant throughout the day. At a given time during the day, the water content within a deeper layer tended to be larger than that within a shallower layer.

In contrast, for a wet day, the water content within the surface layer was increased as a result of rainfall (Fig. 10). If the rainfall was large, the water content within the 10-cm or a deeper layer could also be increased. The maximum water content within the surface or 10-cm layer occurred during the rainfall event, while the maximum water content within a deeper layer appeared sometime after the cease of the rain, probably resulting from the redistribution of soil water of infiltration.

3.4. The simulated soil evaporation

For a given non-rainy day, the peak evaporation rate occurred around 9:30 a.m. in January to May and September to November, while it occurred around 1:00 p.m. in June to August and December (Fig. 11). The evaporation primarily caused decrease of water content in Layer 1 (i.e., the top 5 cm soils), indicating that this soil layer was the major evaporation zone before the peak time. After the peak time, the water content in Layer 1 kept on decreasing until it reached a minimum in late afternoon (i.e., around 2:00 to 3:00 p.m.), after which the water content started to increase. This indicates that Layer 1 might function as an evaporation zone before 9:30 a.m. or 1:00 p.m., depending on the month of interest, while it could function as a condensation/storage zone after 3:00 p.m., regardless of the month of interest. In late afternoon, the thermal gradient might become upward positive, causing upward liquid/vapor fluxes from the deeper layers to replenish soil water in Layer 1. The upward vapor from the deeper soil layers might roughly compensate the evaporation at a given time, while some of the upward vapor could be condensed into liquid water. The condensed liquid water and the upward liquid water from the deeper layers might be stored in Layer 1, causing the increase of water content in this layer. Such a process of evaporation, thermal upward fluxing, condensation, and storing might be the major characteristic of hydrologic cycle at the study site. The negligible fluctuation of water content in Layer 2 (i.e.,

the 5–10 cm soils) and Layer 3 (i.e., the 10–15 cm soils) indicates that the upward thermal liquid flux might be almost same as the vaporization rate in these two layers. Based on Tables 5 and 6, in late afternoon, the vaporization probably occurred around the 10 cm depth, below which the vapor flux was very small. As expected, for a given time, the evaporation rate was much higher on a day in June to September than in other months.

For a given rainy day, the evaporation rate started to decrease from the inception of rain onward, reached a minimum value at the end of rain, and then started to gradually increase (Fig. 12). This indicates that during rainfall event, the potential evapotranspiration might be greatly lowered, which in turn limited the actual evaporation though relatively more water could be available for evaporation. Because the soils at the study site are highly permeable ($K_s = 650 \text{ cm d}^{-1}$ in Table 2), the rain water could quickly infiltrate into Layers 1 and 2, as indicated by the synchronic increase of water content in these two layers during raining. However, the water content in Layer 3 was almost constant and seemed not to be influenced by rain. That is, for most of the rainy days, the rainfall could more often replenish the top 10 cm soils most of the time, and might less often wet the deeper soils and recharge the shallow groundwater, which can be further verified by the negative or small positive changes of water content in the deeper layers as well as the negative or small positive values of deep percolation. The diurnal variations of evaporation rate and water content in a rainy day were mainly controlled by the rain pattern (i.e., timing, amount, and duration), which is distinctly different from those in a non-rainy day.

4. Discussion

Generally, water vapor flow plays a critical role in assessment of the physical processes related to soil heating, distribution of water, and water vapor exchange between the soil and its ambient atmosphere. In desert environment, because the evaporation demand is much greater than the amount of available water, soil water vaporization often occurs at some depth (> 10 cm in our study) below the ground surface and thus the pore vapor needs to be transported by an upward positive heat gradient through the upper dry soils into the ambient atmosphere

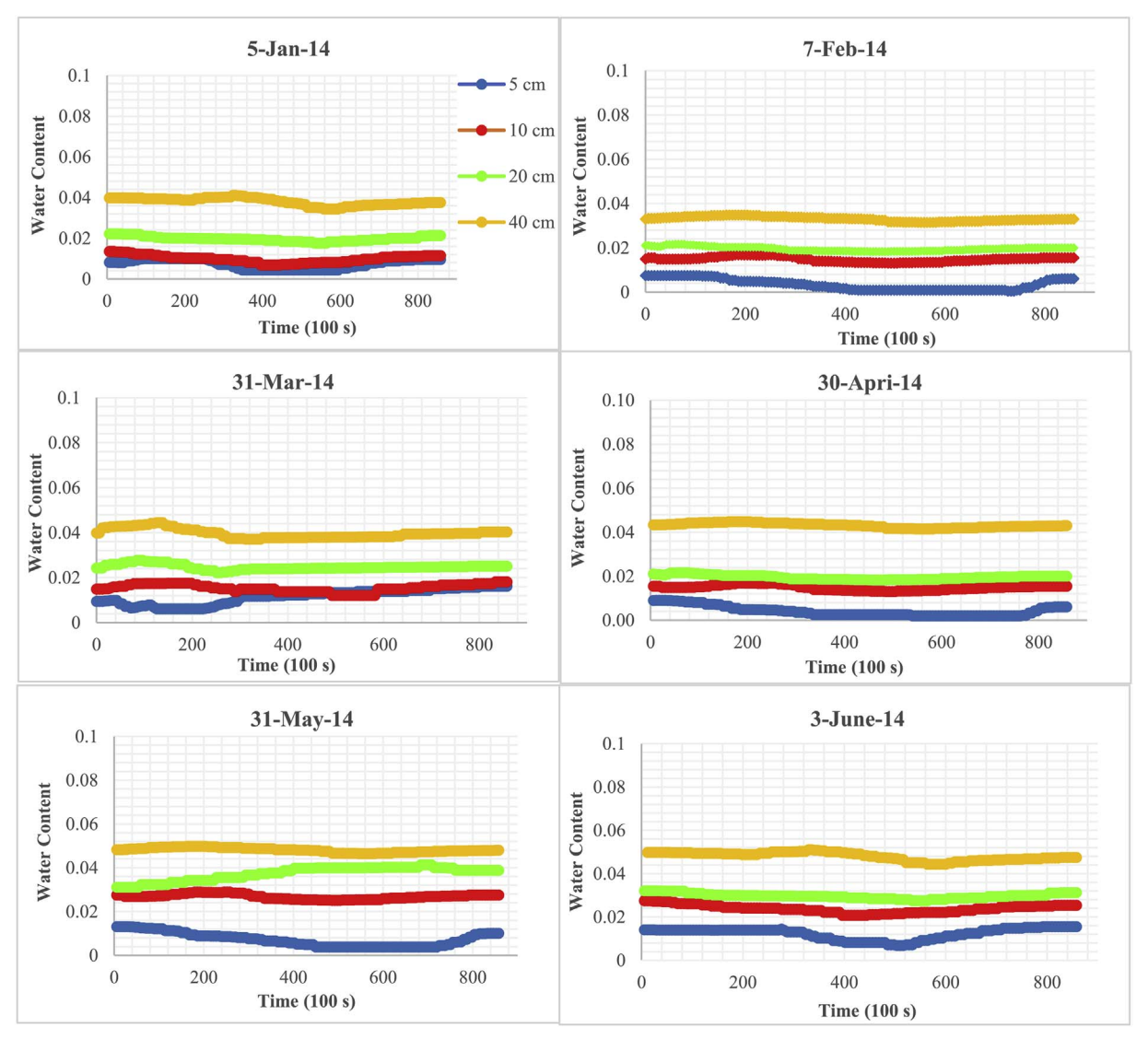


Fig. 9. The simulated diurnal variations of volumetric water content within the soil layers for the same dry days as those in Fig. 7.

(Wang, 2015). Such a soil water evaporation process has yet been fully understood and barely described by existing evaporation models, including the most widely-used Penman-Monteith model (Monteith, 1965). This knowledge gap can limit human's capability to take cost-effective measures to sustain the fragile desert ecosystems as well as will likely bias the prediction of global climate change because such ecosystems account for more than 20% of the earth's terrestrial surface and are distributed across the continents. Our study attempts to understand the dynamics of soil water and pore vapor using the measured data and HYDRUS-1D model at a site located within the typical desert environment of HSL.

Our study used the latest HYDRUS-1D code to produce the diurnal profiles of pore relative humidity (RH $_{\rm pa}$) and soil water content (SWC). The results show that the fluctuation of soil temperature tended to decrease with depth and that the surface soil temperature had a maximum diurnal variation. At the depth of 60 cm, the variation of soil temperature was less than 2 $^{\circ}$ C. The soil temperature gradient, defined as the derivative of soil temperature in respect to vertical distance, was steepest at a depth of around 10 cm, at which the maximum thermal vapor flux was maximal (Fig. 13). This indicates that at this depth, the heat exchange was most active and the primary vaporization occurred (Wang, 2015). In addition, for non-rainy days, the relative magnitude of atmosphere temperature ($T_{\rm atm}$) versus soil temperature determines the

diurnal variations of RH_{pa} and SWC in the top 10 cm soils (Fig. 11), whereas, for rainy days, the rainfall pattern controls the diurnal variations (Fig. 12). For the soils deeper than 10 cm, the RHpa and SWC have a negligible diurnal variation on both non-rainy and rainy days, indicating that the upper boundary conditions may mainly affect the dynamics of soil water and vapor within the top 10 cm soils. For a given non-rainy day, the RH_{pa} and SWC in the top 5 cm soils tended to decrease with increase of Tatm, become minimal around 2:00 p.m. when Tatm was probably warmest, and then increase with decrease of Tatm (Figs. 6 and 7). This is consistent with the finding of Goss and Madliger (2007). The possible reason is that the top 5 cm soils are mostly dry and have a temperature either close to or higher than T_{atm} at any time within the day. As a result, the soil water and pore vapor in the top 5 cm soils can be more quickly moved up into the ambient atmosphere around 2:00 p.m., when the solar radiation is maximal, than at other times, when the solar radiation becomes relatively smaller.

In contrast, in the soils between 5 and 10 cm, the $\rm RH_{pa}$ reached a maximum around 2:00 p.m. and then reduced to a smaller value, whereas, the SWC was almost invariant. One possible reason is that around 2:00 p.m. the temperature of the 5 cm soils was higher than that of the 5–10 cm soils, resulting in a downward positive temperature gradient, retarding the upward movement of vapor (Equation (4)). Another possible reason is that around 2:00 p.m., more heat (from solar

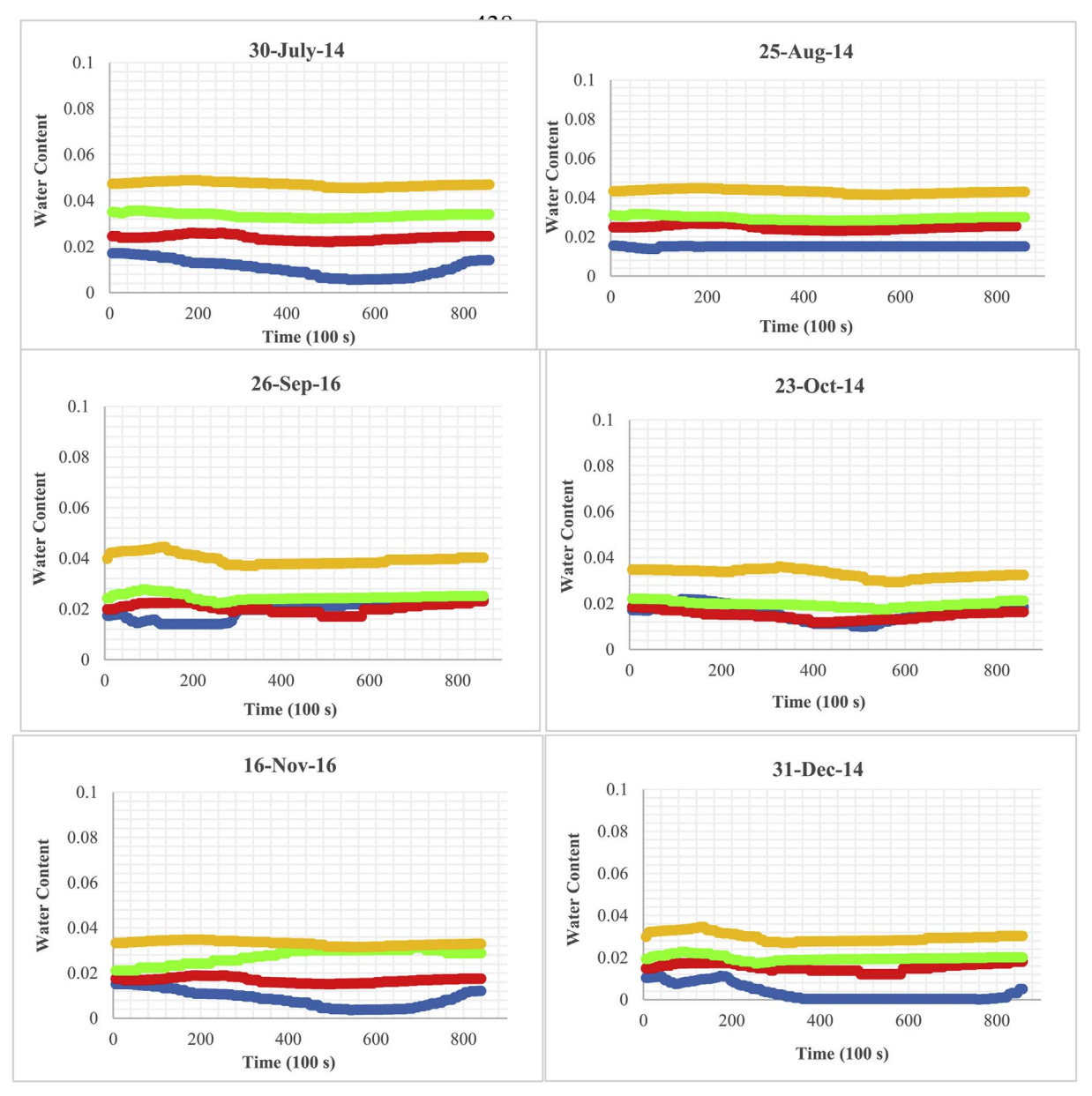


Fig. 9. (continued)

radiation) was transferred down into the soils, vaporizing more soil water. At other times, because $T_{\rm atm}$ probably became lower than the temperature of the soils between 5 and 10 cm, the downward positive temperature gradient could be reversed to an upward positive gradient and thus the cumulated vapor could be moved up through the 5 cm soils into the ambient atmosphere, causing the decrease of RH_{pa} . Our results indicate that in dry days, the RH_{pa} was minimal at midnight, when the total heat flux out of the soils was greatest, while it reached a maximum around 2:00 p.m., when the total heat flux into the soils was largest. This is a typical feature of Phase III evaporation, which has a very low but near-constant evaporation rate, as discussed above. Note that for Phase III, some vapor near the soil surface could be condensed into liquid water, replenishing the top 5 cm soils as shown in Fig. 8, if $T_{\rm atm}$ is lower than the dew point temperature and/or the actual vapor pressure is larger than the saturated vapor pressure (Viessman and Lewis, 2003).

For a rainy day, the RH_{pa} and SWC in the top 5 cm soils reached a peak during the rainfall period (Figs. 8 and 10). As a result of the rain, the soil evaporation could be switched from Phase III either to Phase II or Phase I (Wang, 2015). At these two latter phases, vaporization mainly occurs near the soil surface. However, as the progress of

vaporization, a DSL can be formed again, switching soil evaporation back to Phase III again. In comparison with that for a non-rainy day, the RH $_{\rm pa}$ in the soils between 5 and 10 cm had a much smaller variation (Fig. 7 versus Fig. 8). One possible reason is that in a rainy day, $T_{\rm atm}$ was cooler, leading to a smaller downward temperature gradient and thus less retardation to the upward movement of vapor. Another possible reason is that less heat might be transferred into the soils to vaporize the soil water. Moreover, the higher atmosphere humidity could increase the chance for vapor in the ambient atmosphere to be condensed to replenish soil water in the top 5 cm soils, while it could also retard the movement of pore vapor up into the ambient atmosphere.

At the annual time scale, for the non-rainy days, the average RH_{pa} in the surface soil layer was slightly higher in 2014 (48.88%) than 2013 (45.57%), in a deeper layer, however, the RH_{pa} was literally same (Table 5a versus 5b). For the rainy days, regardless of the soil layer, the average RH_{pa} was same for both years. This indicates that the increased precipitation in 2014 (Table 1) had a minimal influence on the pore vapor within the soils. The higher RH_{pa} in the surface soil layer for the non-rainy days was probably resulted from the condensation of vapor from the ambient atmosphere (McHugh et al., 2015) because year 2014

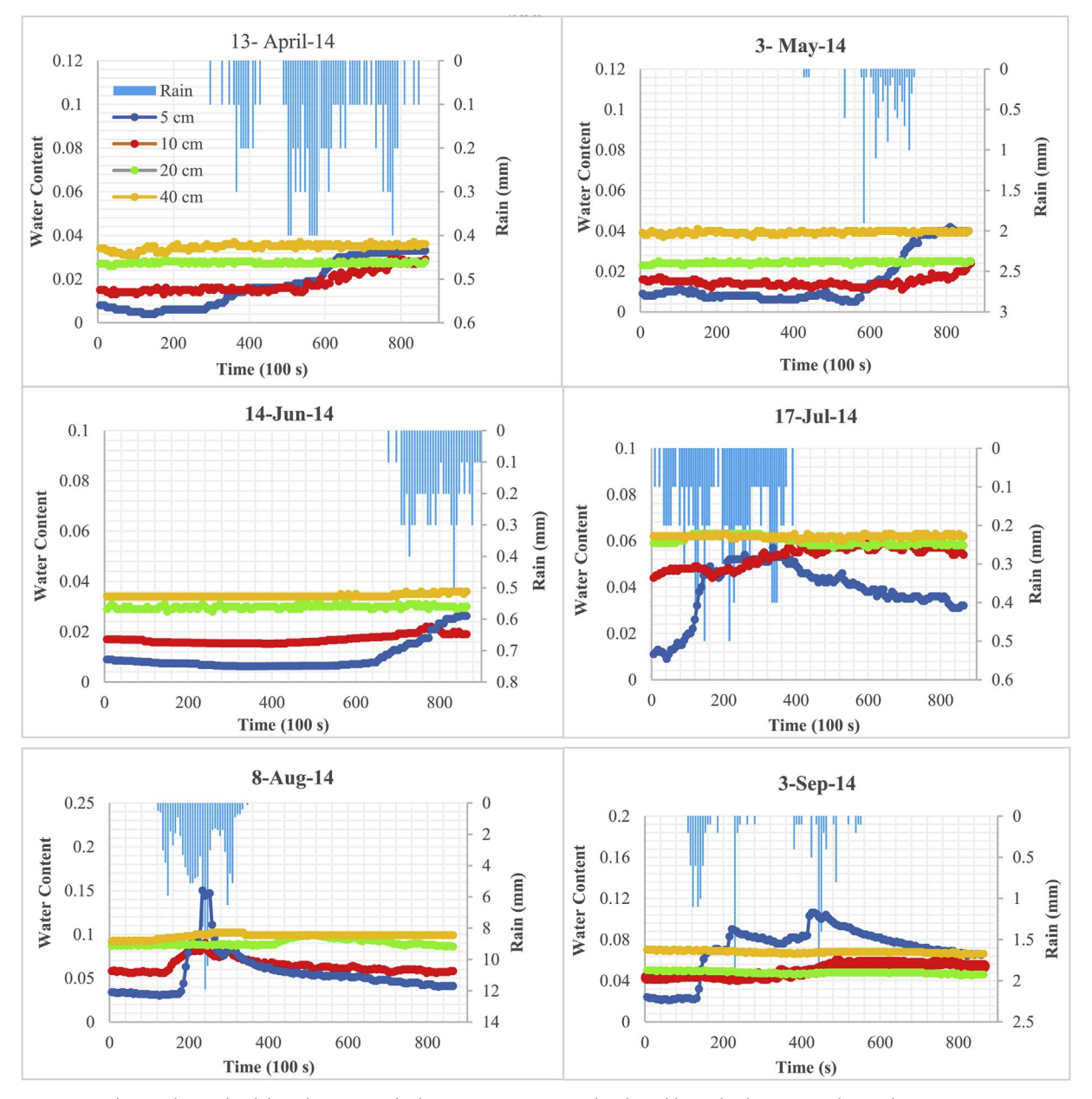
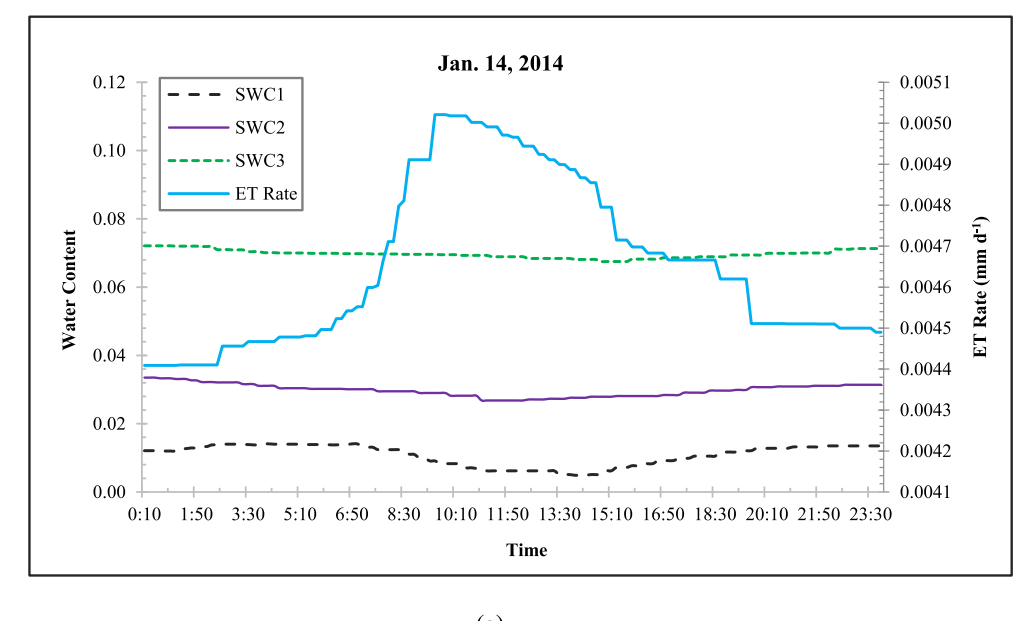


Fig. 10. The simulated diurnal variations of volumetric water content within the soil layers for the same wet days as those in Fig. 8.

was more humid, and thus had a larger air relative humidity, than year 2013. In contrast, at the monthly time scale, for the months of July to November, regardless of the non-rainy or rany days, the increased precipitation in 2014 (Table 1 and Figs. 1 and 2) did result in a higher RH_{pa} within any soil layer (Table 5a versus 5b). The total precipitation of these five months in 2014 was 96.5 mm more than that in 2013, most of which might be converted into pore vapor. For the other months, the increased precipitation in 2014 caused the RH_{pa} to increase in a month but decrease in another month, regardless of the non-rainy or rainy days. One possible reason is that the latent heat for vaporization was less in 2014 because of the more rainy days. Another possible reason is that the cooler air temperature could prompt the emission of pore vapor into the ambient atmosphere, leading to the decrease of RHpa within the soils. On the other hand, as expected and overall, the SWC was higher in 2014 than 2013 regardless of the time scales, soil layers, and non-rainy or rainy days (Table 6a versus 6b). This indicates that more precipitation is always beneficial to infiltration and replenishment of soil moisture. For a given month and a soil layer, the SWC increase from 2013 to 2014 was mainly dependent on the increase of precipitation

intensity rather than that of total precipitation. Herein, precipitation intensity is defined as the ratio of total precipitation to number of rainy days. For instance, while the increase of monthly precipitation in August was larger than that in July (44.3 ersus 24.3 mm) (Table 1), the SWC increase in August was smaller. The increase of precipitation intensity in August was almost half smaller than that in July (13.3 versus 26.2 mm d $^{-1}$). The reason is that because of the very high evaporation rate at the study site, more of the precipitation with a smaller intensity tends to be evaporated before reaching the ground (Viessman and Lewis, 2003), remaining less water for infiltration and replenishing soil moisture.

Our results are consistent with those reported by others (Kobayashi et al., 1989; Goss and Madliger, 2007; Han and Zhou, 2013). Using Rotronic Hygroclip (RH) SC04 probes, Goss and Madliger (2007) measured T_{atm} and RH_{pa} in pore air of dry sandy soils at a Tanzanian site (6°51′S, 37°38′E) for an observation period of consecutive 30 days. The measured data indicate that for a typical day, during Phase I and II, RH_{pa} increases with increase of T_{atm} (reaching a maximum value around noon) regardless of soil depth, during Phase III, however, RH_{pa}



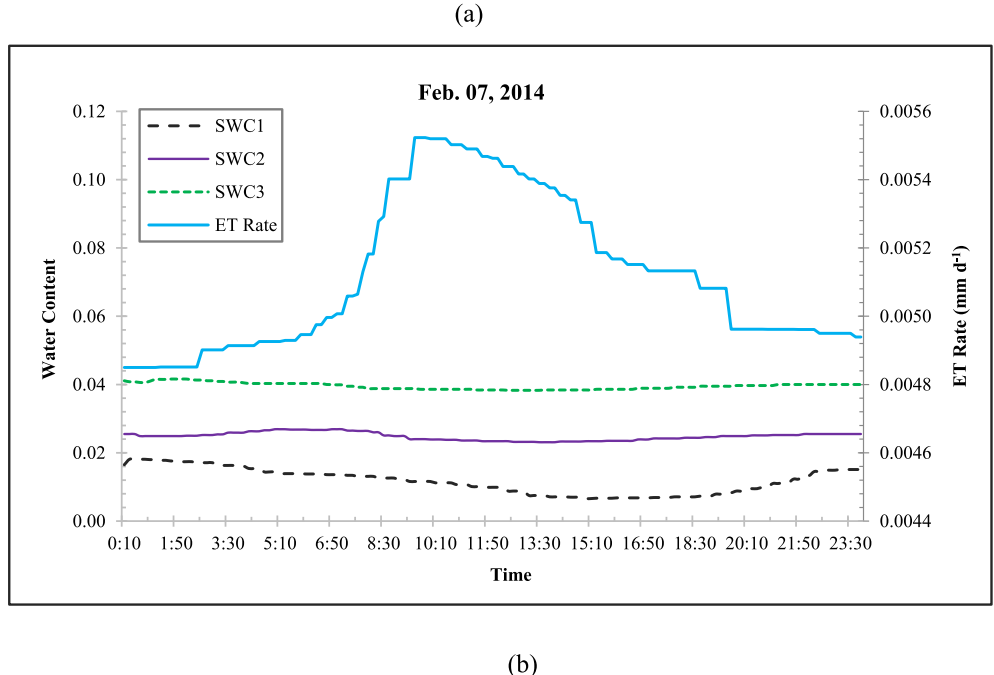
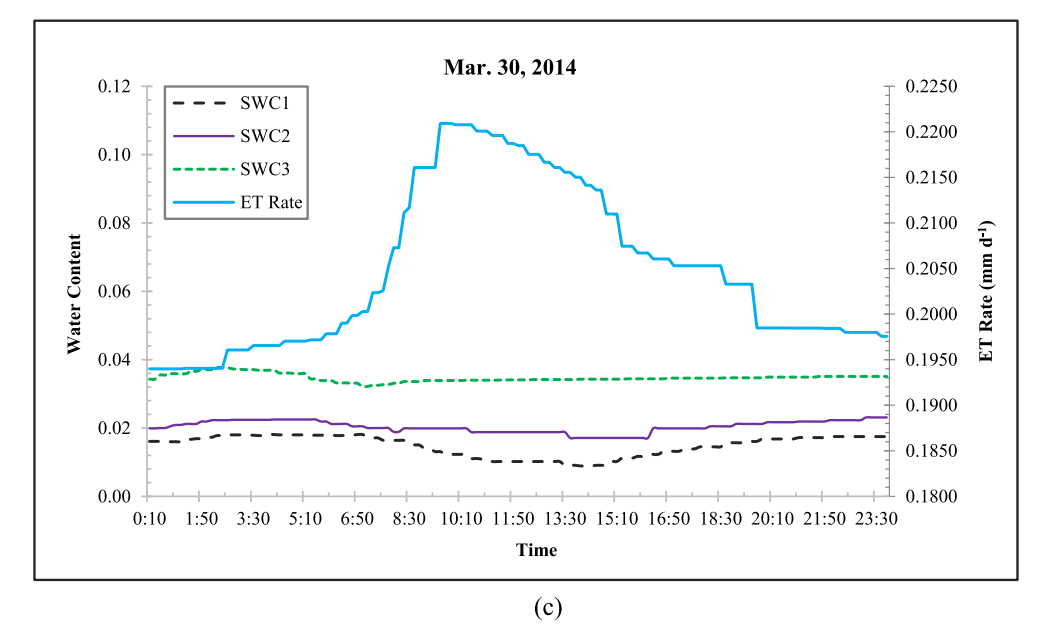


Fig. 11. The simulated evaporation (ET) rate and water content in Layer 1 (SWC1), Layer 2 (SWC2), and Layer 3 (SWC3) on selected dry (i.e., non-rainy) days. Layers 1, 2, and 3 are defined as 0-5, 5-10, and 10-20 cm soils, respectively.

decreases with increase of T_{atm} for the top DSL (reaching a minimum value around noon) but increases with increase of Tatm for the evaporation zone (reaching a maximum value around noon). The data also indicate that continuous evaporation tends to move the evaporation zone down into a deeper soil layer (i.e., increase the thickness of top DSL) but sporadic rain can bring the evaporation zone up back to a shallower soil layer (i.e., reduce the thickness of top DSL). Our simulated values of SWC (Tables 6a and 6b) are comparable with those in other deserted lands (e.g., Namib Desert and Negev Desert). In an observation study conducted in a 30 km² dune field located within the Negev Desert, where the average annual precipitation ranges from 70 to 150 mm, Zaady et al. (2014) found that the soil moisture varied from 0.025 to 0.08, depending on the soil infiltration rate and rainfall gradient (i.e., intensity). Using observed data at three sites within the Namib Desert, where the average annual precipitation ranges from 5 to 100 mm, Li et al. (2016b) developed and used a stochastic model to examine the effect of rainfall on soil moisture. They found that the soil moisture varied from 0.0045 to 0.037 and was controlled by rainfall pattern as well as fog and dew. Although the precipitation at our study site is slightly larger than that in the Namib Desert and Negev Desert, the soil moisture levels at all three locations are not uncompatible. One possible explanation is that the repellent impact of DSL can prevent the beneath moist soils from being further dried up (Wang, 2015). Another possible explanation is that vapor in the overlying atmosphere can be condensed to replenish moisture of the (especially top 5 cm) soils (Zaady et al., 2014; McHugh et al., 2015).

In this study, we focused on the temporal variations of SWC and $RH_{\rm pa}$ at various depths of interest, while also we examined the vertical thermal fluxes of vapor. Our results have practical implications for restoring and/or protecting fragile ecosystems of desert lands across the world, which are characterized by high solar radiation, prevalent and high-speed wind, low atmospheric humidity, and sporadic and low-



Apr. 30, 2014 0.12 0.4600 SWC1 SWC2 0.4400 0.10 ·· SWC3 ET Rate 0.4200 0.08 Water Content 0.4000 0.06 0.3800 0.04 0.3600 0.02 0.3400 0.00 0.3200 1:50 3:30 5:10 6:50 8:30 10:10 11:50 13:30 15:10 16:50 18:30 20:10 21:50 23:30 Time (d)

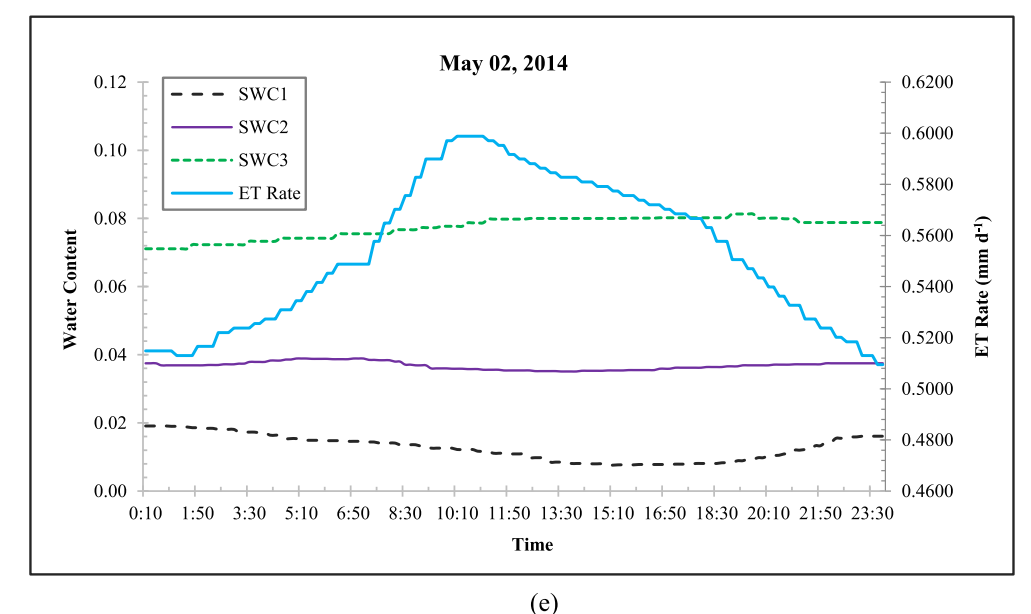
Fig. 11. (continued)

magnitude precipitation. In desert environment, because the climatic evaporation demand is usually much greater than the available surface water, soil water is evaporated to meet the evaporation demand deficit. However, the evaporation process of soil water can be effectively retarded by the top DSL (with an albedo of 0.4 or larger), which can reflect much of solar radiation back into the atmosphere and thus reducing the heat to be transferred into the beneath moist soils. As a result, the moist soils can be protected by the top DSL from being further dried up. In the past decades, because of the incomplete understanding of the retardation role of such a DSL, trees had been planted as a malpractice to prevent dust winds and improve desert ecosystems (Wang et al., 2016). The roots of trees can penetrate through the top DSL into beneath moist soils to transpire a large amount of water, drying up the moist soils. As the growth of trees, the roots will penetrate into, and dry up, deeper moist soils, greatly increasing the thickness of dry soils. At some point, the moist soils will be buried by dry soils too deep to be reached by the roots and trees will start to die off, leading to a worse ecoenvironment. In terms of our results, we recommend that native sand-fixing plants (e.g., Salsolar tragus, Salix gordejevii, and

Caragana microphylla) (Duan et al., 2017), which have roots not penetrating into deep moist soils (i.e., a root depth of around 10 cm), do not transpire much soil water ($< 2.8 \text{ mm d}^{-1}$), and can stabilize the top DSL, be planted to restore/protect desert ecosystems. Such plants have needle-shaped leaves with a very small leaf area index and can close their leaf stomata when water is not sufficient for transpiration. Their roots can capture, store, and utilize soil water from sources of infiltration, capillary rise, and vapor condensation from the overlying air (McHugh et al., 2015). The vegetation species of Salsolar tragus, Salix gordejevii, and Caragana microphylla are native to, and currently exist in, the study area (Duan et al., 2017).

5. Conclusions

This study examined the dynamics of soil water and pore vapor in the dry sandy soils at a typical site within the Horqin Sandy Land (HSL). The examination was done using a HYDRUS-1D model that was calibrated and validated using the measured data on climate and soil water in 2013 and 2014. The results revealed a threshold depth of 10 cm,



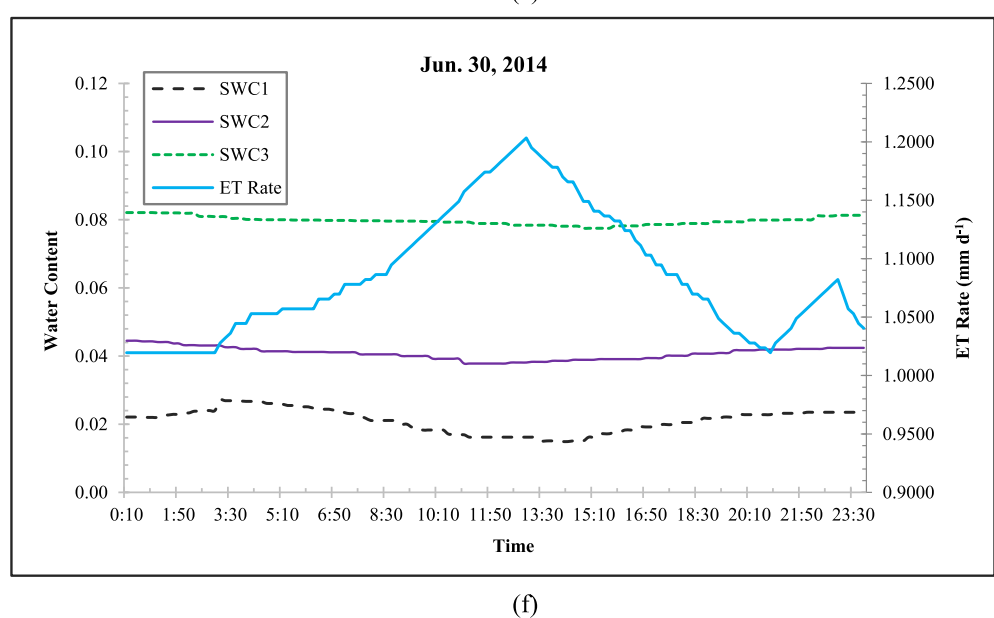


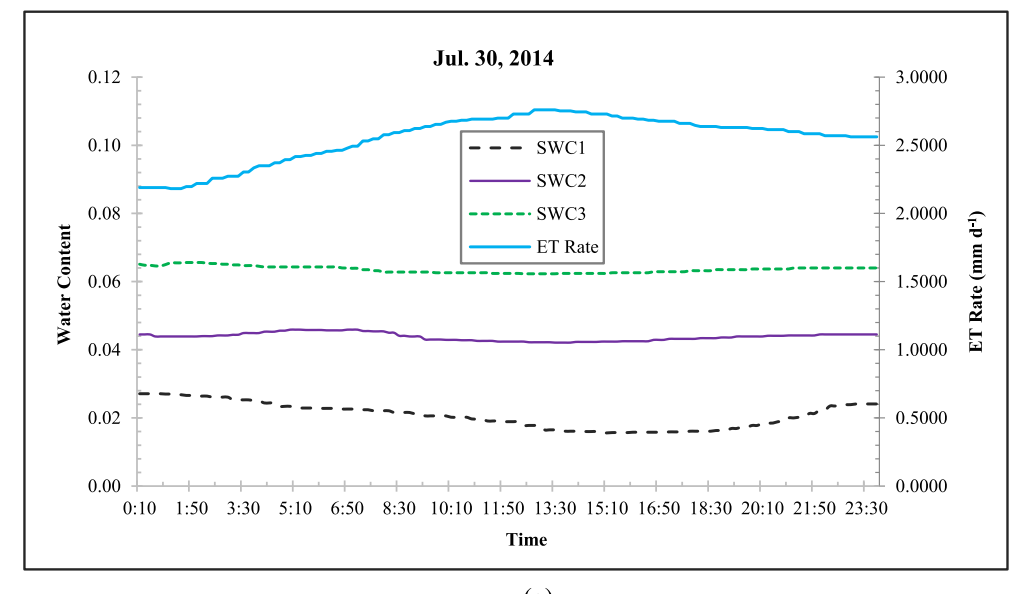
Fig. 11. (continued)

below which the soils had almost constant soil water content (SWC) and pore air relative humidity (RH $_{\rm pa}$). For a given non-rainy day, the RH $_{\rm pa}$ and SWC in the top 5 cm soils tended to decrease with increase of atmosphere temperature (T $_{\rm atm}$), attaining a minimum around 2:00 p.m. In the soils between 5 and 10 cm, the SWC had a negligible diurnal variation, whereas, the RH $_{\rm pa}$ tended to increase with increase of T $_{\rm atm}$. In contrast, for a rainy day, the diurnal variations of RH $_{\rm pa}$ and SWC in the top 10 cm soils were mainly controlled by the rainfall pattern and amount, with maximums at a time during the rain event. Moreover, the top dry soil layer (DSL) can effectively retard the beneath moist soils from being further dried up. Planting native vegetation that have a shallow root depth (\sim 10 cm) may be preferred to enhance the DSL role in protecting the fragile desert ecosystem.

Acknowledgments

This study was financially supported by the following contracts: the U.S. National Science Foundation (NSF) International Research Experience for Students (IRES) program (# 100653-010); the National Natural Science Foundation of China Basic Research Program:

Hydrological Processes and Ecological Responses (#51139002); the Chinese Ministry of Education "Innovation Team Building Program" Cold-Arid Region Hydrological Processes and Ecoenvironmental Responses (#IRT13069); the Inner Mongolia Autonomous Region Science and Technology Bureau's Major Basic Research Open Project for Oversea Excellent Scholars (#206202057); the Inner Mongolia Agricultural University (IMAU) Innovation Team Building Program Cold-Arid Region Water Resources Utilization (#NDTD2010-6); the International Collaboration Agreement (#5CEC3) between Old Dominion University (ODU) and IMAU; and a research project of the Inner Mongolia Autonomous Region Water Resources Department. Some data were provided by the IMAU Innovation Team Building Program Cold-Arid Region Water Resources Utilization Laboratory and Agula Ecohydrological Experiment Station (AEES). Also, this study was supported by the 2014 Faculty Proposal Preparation Program (FP3-2014) at ODU. Our appreciations are also extended to Ms. Yueying Wang, a native English speaker and biochemistry undergraduate research assistant at Virginia Polytechnic Institute and State University, Blacksburg, Virginia, USA, for her proof editing. Moreover, we highly appreciate the invaluable comments of the two anonymous reviewers.



(g)

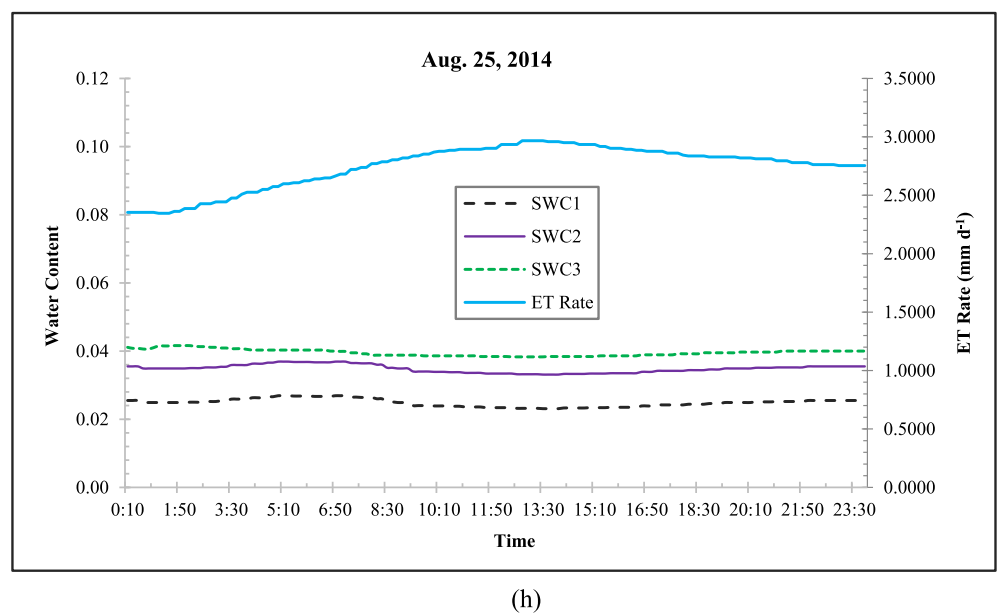
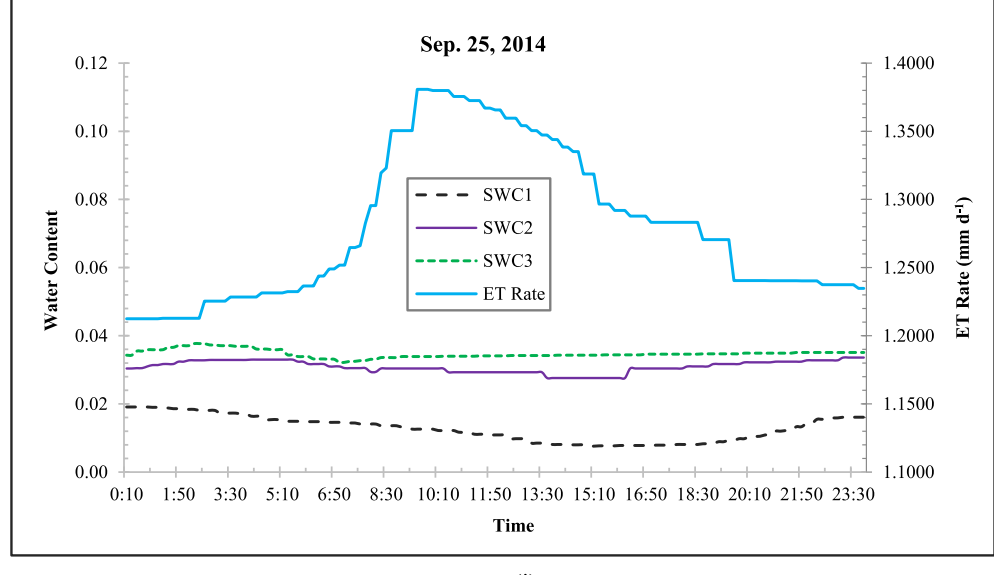


Fig. 11. (continued)



(i)

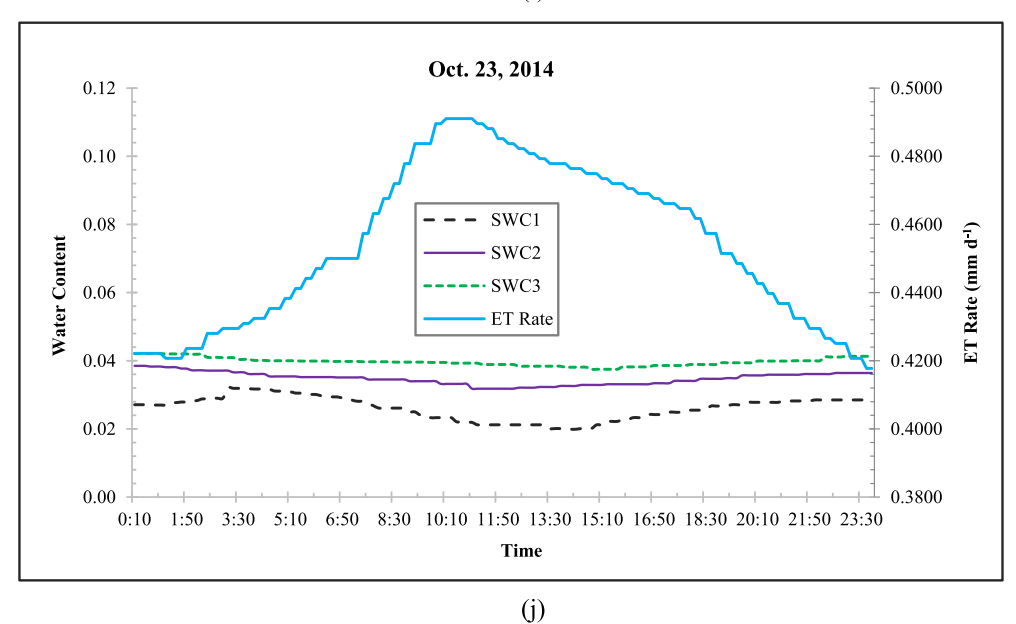
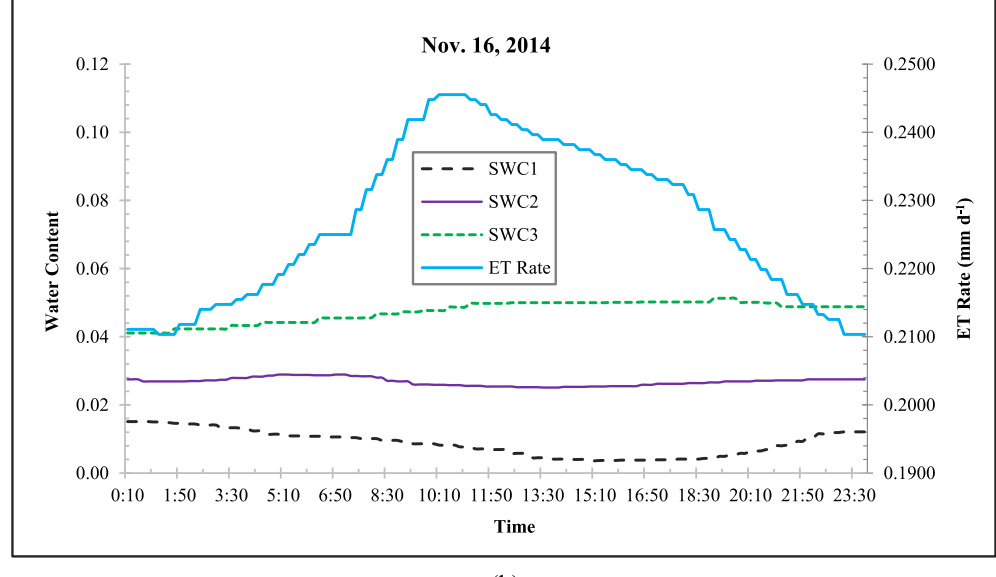


Fig. 11. (continued)



(k)

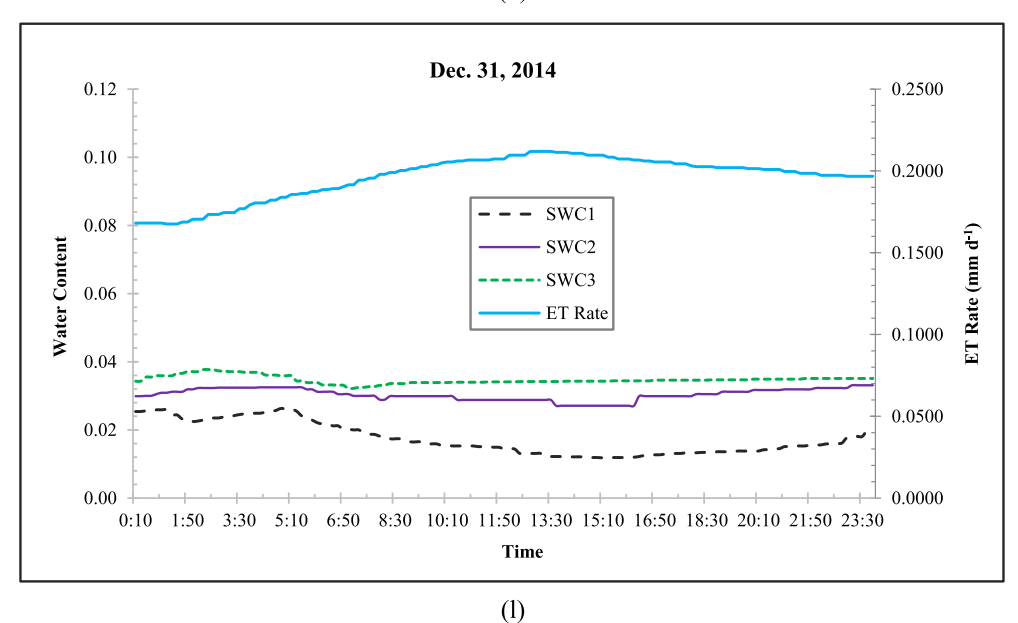
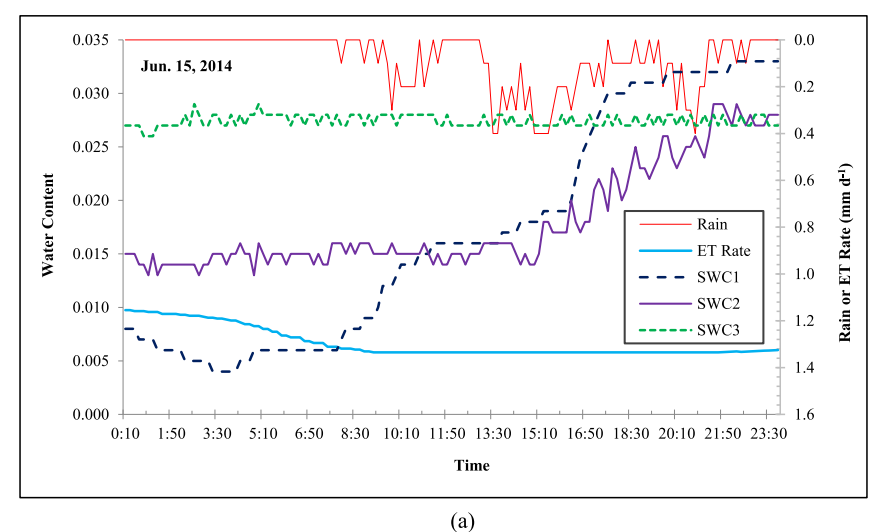
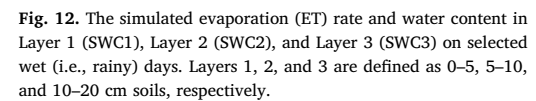
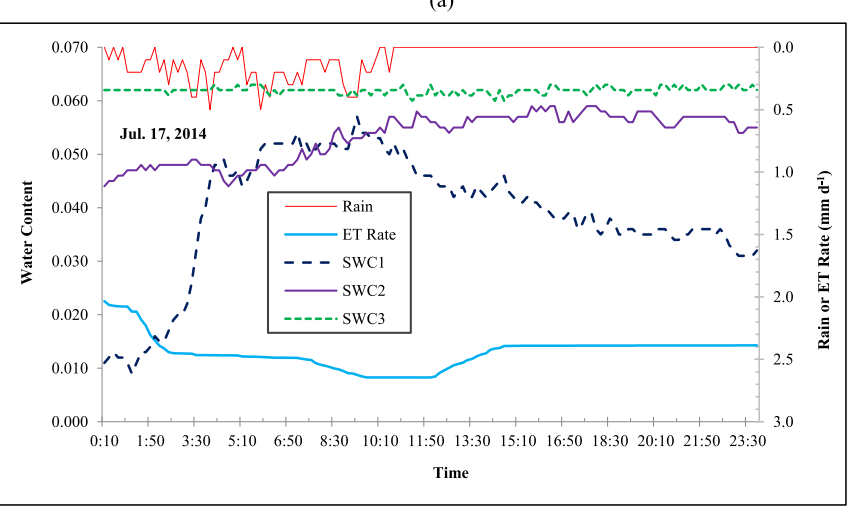


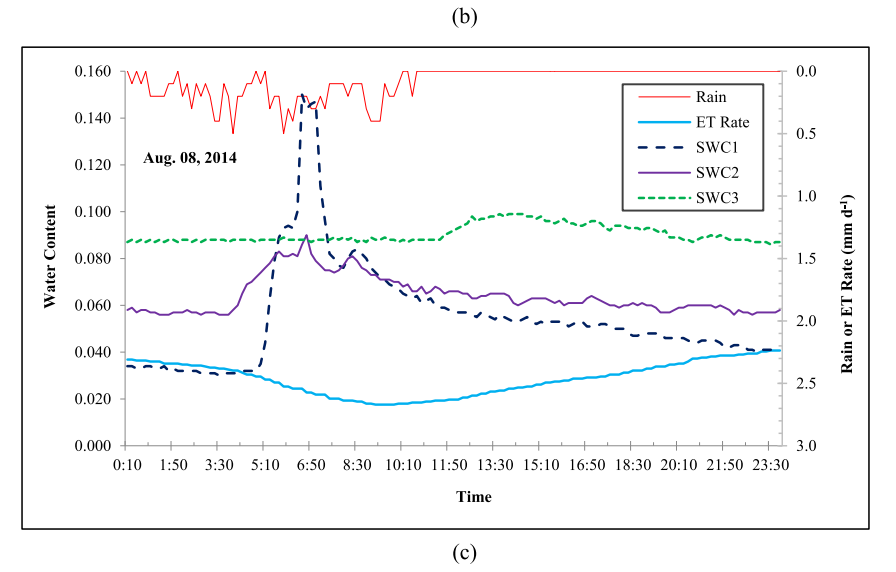
Fig. 11. (continued)

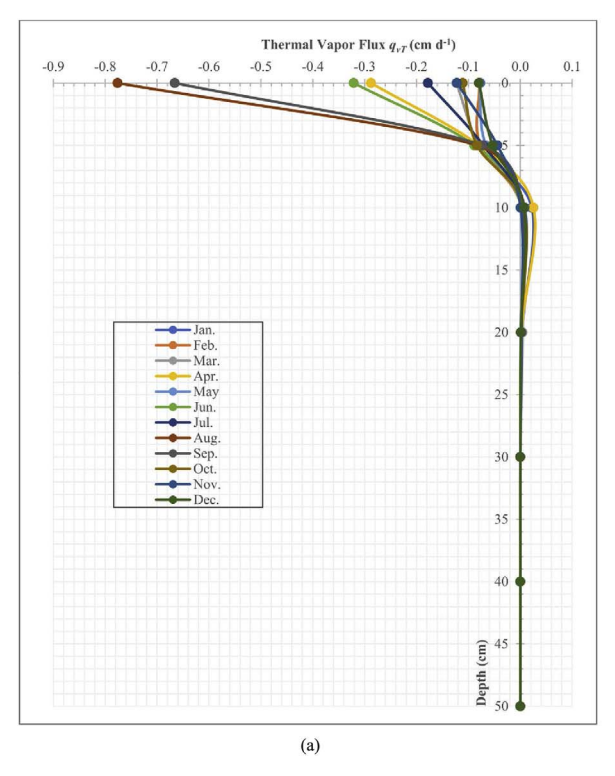
S. Pedram et al.











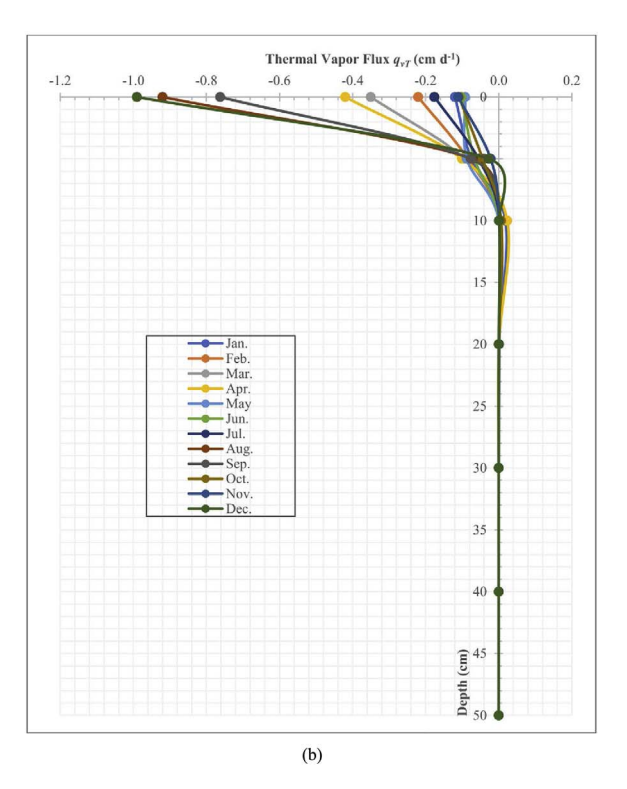


Fig. 13. The simulated thermal vapor flux profiles for: (a) 2013; and (b) 2014.

References

- Bristow, K.L., Campbell, G.S., Calissendorff, K., 1993. Test of a heat-pulse probe for measuring changes in soil water content. Soil Sci. Am. J. 57 (4), 930–934.
- Bristow, K.L., Horton, R., 1996. Modeling the impact of partial surface mulch on soil heat and water flow. Theor. Appl. Climatol. 54, 85–98.
- Daamen, C.C., Simmonds, L.P., 1996. Measurement of evaporation from bare soil and its estimation using surface resistance. Water Resour. Res. 32, 1393–1402.
- Dong, W., Yu, Z., Weber, D., 2003. Simulations on soil water variation in arid regions. J. Hydrol. 275 (3–4), 162–181.
- Duan, L., Liu, T., Wang, X., Luo, Y., 2015. Spatio-temporal patterns of water table and vegetation status of a deserted area. Water 7, 5788–5805. http://dx.doi.org/10. 3390/w7105788
- Duan, L., Liu, T., Wang, X., Wang, G., Ma, L., Luo, Y., 2011. Spatio-temporal variations in soil moisture and physicochemical properties of a typical semiarid sand-meadowdesert landscape as influenced by land use. Hydrol. Earth Syst. Sci. 15, 1865–1877. http://dx.doi.org/10.5194/hess-15-1865-2011.
- Duan, L., Lv, Y., Yan, X., Liu, T., Wang, X., 2017. Upscaling stem to community-level transpiration for two sand-fixing plants: Salix gordejevii and *Caragana microphylla*. Water 9, 361. http://dx.doi.org/10.3390/w9050361.
- Farouki, O.T., 1981. Thermal Properties of Soils. CRREL Monograph 81-1. United States Army Corps of Engineers (USACE) Cold Regions Research and Engineering Laboratory (CRREL), Hanover, NH, pp. 147.
- Ghanbarian-Alavijeh, B., Liaghat, A., Huang, G., van Genuchten, M.Th, 2010. Estimation of the van Genuchten soil water retention properties from soil textural data. Pedosphere 20 (4), 456–465.
- Goss, K., Madliger, M., 2007. Estimation of water transport based on in situ measurements of relative humidity and temperature in a dry Tanzanian soil. Water Resour. Res. 43, W05433. http://dx.doi.org/10.1029/2006WR005197.
- Gowing, J.W., Konukcu, F., Rose, D.A., 2006. Evaporative flux from a shallow water table: the influence of a vapour-liquid phase transition. J. Hydrol. 321, 77–89.
- Han, J., Zhou, Z., 2013. Dynamics of soil water evaporation during soil drying: laboratory Experiment and Numerical Analysis. Sci. World J. http://dx.doi.org/10.1155/2013/ 240280
- Heitman, J.L., Horton, R., Sauer, T.J., DeSutter, T.M., 2008. Sensible heat observations reveal soil-water evaporation dynamics. J. Hydrometeorol. 9, 165–171.
- Kamai, T., 2013. Development of Heat Pulse Sensors to Measure Vadose Zone Thermal Properties, Water Content, and Water Flux Density. Dissertation. Library at University of California-Davis. Davis. CA.
- Kassas, M., 1995. Desertification: a general review. J. Arid Environ. 30, 115–128.
- Kobayashi, T., Matsuda, A., Kamichika, M., 1989. A simple method for estimating the rate of evaporation from a dry sand surface. J. Agric. Meteorol. 44, 269–274.
- Kondo, J., Saigusa, N., Sato, T., 1992. A model and experimental study of evaporation from bare-soil surfaces. J. Appl. Meteorol. 31, 304–312.
- Li, B., Wang, L., Kaseke, K.F., Li, L., Seely, M.K., 2016b. The impact of rainfall on soil moisture dynamics in a foggy desert. PLoS One 11 (10), e0164982. http://dx.doi.org/ 10.1371/journal.pone.0164982.

- Li, Q., Zhang, C., Shen, Y., Jia, W., Li, J., 2016a. Quantitative assessment of the relative roles of climate change and human activities in desertification processes on the Qinghai-Tibet Plateau based on net primary productivity. Catena 147, 789–796.
- Liu, G., Wen, M., Chang, X., Ren, T., Horton, R., 2013. A self-calibrated dual probe heat pulse sensor for in situ calibrating the probe spacing. Soil Sci. Soc. Am. J. 77 (2), 417–421. http://dx.doi.org/10.2136/sssaj2012.0434n.
- Liu, X., 2011. Evaluation of the heat-pulse technique for measuring soil water content with thermo-TDR sensor. Procedia Environ. Sci. 11, 1234–1239.
- Mahfouf, J.F., Noilhan, J., 1991. Comparative study of various formulations of evaporation from bare soil using in situ data. J. Appl. Meteorol. 30, 1354–1365.
- McHugh, T.A., Morrissey, E.M., Reed, S.C., Hungate, B.A., Schwartz, E., 2015. Water from air: an overlooked source of moisture in arid and semiarid regions. Sci. Rep. 5, 13767, http://dx.doi.org/10.1038/srep13767.
- Monteith, J.L., 1965. Evaporation and environment. In state and movement of water in living organisms. In: Proc. 19th Symp. Society of Experimental Biology. Cambridge University Press, Cambridge, U.K., pp. 205–234.
- Mori, Y., Hopmans, J.W., Mortensen, A.P., Kluitenberg, G.J., 2003. Multi-functional heat pulse probe for the simultaneous measurement of soil water content, solute concentration, and heat transport parameters. Vadose Zone J. 2, 561–570.
- Novak, M.D., 2010. Dynamics of the near-surface evaporation zone and corresponding effects on the surface energy balance of a drying bare soil. Agric. For. Meteorol. 150, 1358–1365.
- Philip, J.R., 1958. Evaporation, and moisture and heat fields in the soil. J. Meteorol. 14, 354–366.
- Philip, J.R., de Vries, D.A., 1957. Moisture movement in porous materials under temperature gradients. Trans. Am. Geophys. Union 38, 222–232.
- Saito, H.; Sakai, M.; Toride, N.; Šimůne, K. Advanced modeling of water flow and contaminant transport in porous media using the HYDRUS. Proc. of the Third HYDRUS Workshop, Fuchu Tokyo, Japan. 28 June 2008. Department of Ecoregion Science, Tokyo University of Agriculture & Technology.
- Saito, H., Šimůnek, J., Mohanty, B., 2006. Numerical analyses of coupled water, vapor and heat transport in the vadose zone. Vadose Zone J. 5 (2), 784–800.
- Sakai, M., Jones, S.B., Tuller, M., 2011. Numerical evaluation of subsurface soil water evaporation derived from sensible heat balance. Water Resour. Res. 47, W02547. http://dx.doi.org/10.1029/2010WR009866.
- Saravanapavan, T., Salvucci, G.D., 2000. Analysis of rate-limiting processes in soil evaporation with implications for soil resistance models. Adv. Water Resour. 23, 493–502
- Šejna, M., Šimůnek, J., van Genuchten, M. Th, 2011. The HYDRUS Software Package for Simulating Two- and Three-dimensional Movement of Water, Heat, and Multiple Solutes in Variably-saturated Media. User Manual, Version 2.0, PC Progress. Czech Republic, Prague, pp. 280.
- Shahraeeni, E., Lehmann, P., Or, D., 2012. Coupling of evaporative fluxes from drying porous surfaces with air boundary layer - characteristics of evaporation from discrete pores. Water Resour. Res. http://dx.doi.org/10.1029/2012WR011857.
- Šimůnek, J., van Genuchten, M. Th., Šejna, M., 2011. The HYDRUS Software Package for Simulating Two- and Three-dimensional Movement of Water, Heat, and Multiple Solutes in Variably-saturated Media. Technical Manual, Version 2.0, PC Progress.

- Czech Republic, Prague, pp. 258.
- Šimůnek, J., van Genuchten, M.Th, 2008. Modeling nonequilibrium flow and transport with HYDRUS. Vadose Zone J. http://dx.doi.org/10.2136/VZJ2007.0074. Special Issue "Vadose Zone Modeling" 7(2): 782–797.
- Smits, K.M., Ngo, V.V., Cihan, A., Sakaki, T., Illangasekare, T.H., 2012. An evaluation of models of bare soil evaporation formulated with different land surface boundary condition and assumptions. Water Resour. Res. 48, W12526. http://dx.doi.org/10. 1029/2012WR012113.
- van Bavel, C.H.M., Hillel, D.I., 1976. Calculating potential and actual evaporation from a bare soil surface by simulation of concurrent flow of water and heat. Agric. Meteorol. 17, 453–476.
- van Genuchten, M.Th., 1980. A closed-form equation for predicting the hydraulic conductivity of unsaturated soils. Soil Sci. Soc. Am. J. 44, 892–898.
- Viessman Jr., W., Lewis, G.L., 2003. Introduction to Hydrology, fifth ed. Prentice Hall, Upper Saddle River, NJ.
- Wang, X., 2015. Vapor flow resistance of dry soil layer to soil water evaporation in arid environment: an overview. Water 7, 4552–4574.
- Wang, X., Melesse, A.M., Yang, W., 2006. Influences of potential evapotranspiration estimation methods on SWAT's hydrologic simulation in a northwestern Minnesota watershed. Trans. ASABE 49 (6), 1755–1771.
- Wang, X., Pedram, S., Liu, T., Gao, R., Li, F., Luo, Y., 2016. Estimated grass grazing removal rate in a semiarid Eurasian steppe watershed as influenced by climate. Water 8, 339
- Xiao, X., Horton, R., Sauer, T.J., Heitman, J.L., Ren, T., 2011. Cumulative soil water evaporation as a function of depth and time. Vadose Zone J. 10, 1016–1022.

- Yamanaka, T., Takeda, A., Shimada, J., 1998. Evaporation beneath the soil surface: some observational evidence and numerical experiments. Hydrol. Process. 12, 2193–2203.
- Yamanaka, T., Yonetani, T., 1999. Dynamics of the evaporation zone in dry sandy soils. J. Hydrol. 217, 135–148.
- Zaady, E., Katra, I., Yizhaq, H., Kinast, S., Ashkenazy, Y., 2014. Inferring the impact of rainfall gradient on biocrusts' developmental stage and thus on soil physical structures in sand dunes. Aeolian Res. 13, 81–89.
- Zeng, Y., Su, Z., Wan, L., Wen, J., 2011a. A simulation analysis of the advective effect on evaporation using a two-phase heat mass flow model. Water Resour. Res. 47, 10W10529 18pp.
- Zeng, Y., Su, Z., Wan, L., Wen, J., 2011b. Numerical analysis of air-water-heat flow in unsaturated soil: is it necessary to consider airflow in land surface models. J. Geophys. Res. Atmos. 116, D20107 18.
- Zeng, Y., Su, Z., Wan, L., Yang, Z., Zhang, T., Tian, H., Shi, X., Wang, X., Cao, W., 2009.
 Diurnal pattern of the drying front in desert and its application for determining the effective infiltration. Hydrol. Earth Syst. Sci. 13, 703–714.
- Zhao, Y., Peth, S., Horn, R., Krümmelbein, J., Ketzer, B., Gao, Y., Doerner, J., Bernhofer, C., Peng, X., 2010. Modeling grazing effects on coupled water and heat fluxes in Inner Mongolia grassland. Soil Tillage Res. 109, 75–86.
- Zhao, Y., Si, B., He, H., Xu, J., Peth, S., Horn, R., 2016. Modeling of coupled water and heat transfer in freezing and thawing soils, Inner Mongolia. Water 8 (10), 424. http://dx.doi.org/10.3390/w8100424.
- Zucca, C., Julitta, F., Previtali, F., 2011. Land restoration by fodder shrubs in a semi-arid agro-pastoral area of Morocco. Effects on soils. Catena 87, 306–312.